

Variational Bayesian Multiuser Tracking for Reconfigurable Intelligent Surface Aided MIMO-OFDM Systems

Boyuan Teng, *Student Member, IEEE*, Xiaojun Yuan, *Senior Member, IEEE*,
and Rui Wang, *Senior Member, IEEE*

Abstract

Reconfigurable intelligent surface (RIS) has attracted enormous interest for its potential advantages in assisting both wireless communication and environmental sensing. In this paper, we study a challenging multiuser tracking problem in the multiple-input multiple-output (MIMO) orthogonal frequency division multiplexing (OFDM) system aided by multiple RISs. In particular, we assume that a multi-antenna base station (BS) receives the OFDM symbols from single-antenna users reflected by multiple RISs and tracks the positions of these users. Considering the users' mobility and the blockage of light-of-sight (LoS) paths, we establish a probability transition model to characterize the tracking process, where the geometric constraints between channel parameters and multiuser positions are utilized. We further develop an online message passing algorithm, termed the Bayesian multiuser tracking (BMT) algorithm, to estimate the multiuser positions, the angles-of-arrivals (AoAs) at multiple RISs, and the time delay and the blockage of the LoS path. The Bayesian Cramér Rao bound (BCRB) is derived as the fundamental performance limit of the considered tracking problem. Based on the BCRB, we optimize the passive beamforming (PBF) of the multiple RISs to improve the tracking performance. Simulation results show that the proposed PBF design significantly outperforms the counterpart schemes, and our BMT algorithm can achieve up to centimeter-level tracking accuracy.

Index Terms

B. Teng and X. Yuan are with the National Key Laboratory of Science and Technology on Communications, University of Electronic Science and Technology of China, Chengdu 610000, China (e-mail: byteng@std.uestc.edu.cn; xjyuan@uestc.edu.cn).

R. Wang is with the College of Electronics and Information Engineering, Tongji University, Shanghai 201804, China. R. Wang is also with the Shanghai Institute of Intelligent Science and Technology, Tongji University, Shanghai 201804, China (e-mail: ruiwang@tongji.edu.cn).

User tracking, reconfigurable intelligent surface, MIMO-OFDM, Bayesian inference, passive beamforming.

I. INTRODUCTION

The sixth-generation (6G) mobile communication is expected to provide integrated sensing and communications (ISAC) service to enable emerging applications, such as digital twin, artificial intelligence (AI), virtual reality (VR), internet of vehicles (IoV), etc [1]–[4]. As a critical issue in sensing, the acquisition of high-precision location information enables the interaction between the digital and physical worlds and is indispensable in the implementation of emerging applications [5]. With the carrier frequencies moving towards millimeter-wave (mmWave) and higher sub-THz spectrum, broad bandwidth signals and large antenna arrays will be widely used in 6G, leading to high sensing resolution in the angular and delay domains [6]. Without introducing additional hardware equipment, high-accuracy localization becomes possible based on radio signals.

Common radio localization methods are driven by the measurements of the angle of arrival (AoA), angle of departure (AoD), time of arrival (ToA), and received signal strength (RSS) from radio signals with several base stations (BSs) regarded as reference anchors [5], [6]. In communication, the multipath effect provides spatial multiplexing which increases the communication capability of the channel. However, only the measurements corresponding to the line-of-sight (LoS) paths contribute to localization, and the non-LoS components reflected by scatters are regarded as interference since environment map information is unavailable [7]. Unfortunately, in mobile communication scenarios, due to highly complicated propagation environments, the LoS path may be blocked by obstacles, such that the localization methods fail to work.

To cope with the above issue in localization, reconfigurable intelligent surface (RIS) is deployed in the electromagnetic environment as an energy-efficient and cost-effective device [8]–[11]. A RIS is generally an electromagnetic metasurface composed of a large number of passive reflecting elements that independently modify the incident radio waves by inducing controllable amplitude and additional phase changes [12]. It provides an extra configurable reflecting path to assist both communication and localization. With efficient passive beamforming (PBF) design, the wireless channel fading impairment and interference issue can be mitigated leading to significant communication quality improvement [13], [14]. From the localization point of view, the RIS acts as an extra reference anchor and provides additional measurements to enable localization via a single BS and avoids the reliance on the LoS path [5].

While RIS-aided communication has been extensively investigated, the research on the use of RIS for localization is still in its infancy. Early works are summarized as follows. Based on the RSS measurements, the authors in [15] propose a RIS-aided indoor user positioning scheme where the PBF of RIS is optimized to obtain a high-resolution signal strength map. However, the RSS measurements-based localization schemes rely on an idealized path loss model which is not accurate in practice. In [16] and [17], a 3-dimension (3D) localization system is considered where the channel angle parameters and the user position are estimated based on the maximum likelihood principle. For the multiple-input multiple-output (MIMO) orthogonal frequency division multiplexing (OFDM) systems, the work [18] realizes environment mapping and user localization by using the so-called twin-RIS structure and exploiting array signal processing to acquire the channel parameters. The work [19] proposes a new conformal structure for RIS which enables the estimations of AoDs and AoAs of a RIS. The scatterer and user localization problem is then tackled by combining the delay and angle estimations. The joint localization and synchronization problem is studied in [20], where the BS precoding and the RIS PBF design are optimized based on a novel beamforming codebook. In our prior work [21], we consider a user tracking problem and propose an online Bayesian tracking algorithm based on the AoAs estimation at the user antenna array exploiting the temporal correlation of the user location.

All the above works are limited to the category of single-user localization/tracking. Recently, [22] studies a multiuser localization problem, where two semi-passive RISs, with each element equipped with radio-frequency transceiver hardware, are introduced to estimate the AoAs at RISs and further achieve multiuser localization. However, the deployment of semi-passive RISs requires an expensive hardware overhead, which compromises the cost-effectiveness of using RIS. Moreover, the existing literature adopts the assumption that the LoS paths between RISs and users always exist, which makes the proposed algorithm less practicable since a LoS path is possibly blocked in mobile scenarios.

Motivated by the limitations of the existing work, we study the tracking problem for multiple single-antenna users in a MIMO-OFDM system aided by multiple passive RISs, where the blockage of LoS paths between RISs and users is considered in the tracking process. The main contributions of this paper are as follows:

- For the considered tracking problem, we build a probability transition model to characterize the mobility of users and the live-and-death of the LoS paths between RISs and users caused

by blockages.

- Given the factor graph representation of the probability model, we develop an online message passing algorithm, termed the Bayesian multiuser tracking (BMT) algorithm, to jointly estimate the multiuser positions, the AoAs at the multiple RISs, the time delay of each LoS path, and the existence of LoS paths in every frame. We exploit variational inference and Gaussian approximation to calculate the messages.
- We calculate the Bayesian information matrix (BIM) and derive the Bayesian Cram r Rao bound (BCRB) for the considered multiuser tracking problem. The BCRB provides a theoretic mean square error (MSE) lower bound for the tracking problem.
- Based on the derived BCRB, we optimize the passive beamforming design of multiple RISs to improve the tracking performance. The unknown multiuser positions in the optimization problem are substituted by the estimation in the previous frame. The numerical results show that the proposed PBF design outperforms benchmark schemes in sense of both the BCRB and the root mean square error (RMSE) of our multiuser tracking algorithm.

The remainder of this paper is organized as follows. Section II introduces the multi-RIS aided MIMO-OFDM systems and formulates the multiuser tracking problem. In Section III, we derive the message calculations and develop the Bayesian multiuser tracking algorithm. In Section IV, we analyze the BCRB for the multiuser tracking problem. In Section V, we present the BCRB-based passive beamforming design for the multiple RISs. Numerical results are presented in Section VI, and the paper concludes in Section VII.

Notations: Throughout, vectors and matrices are denoted by bold lowercase letters and bold capital letters, respectively. We use $(\cdot)^T$, $(\cdot)^H$, and $(\cdot)^*$ to denote the operations of transpose, conjugate transpose, and conjugate, respectively. We use $\text{Tr}(\mathbf{X})$ to denote the trace of \mathbf{X} , $\text{Re}\{\mathbf{X}\}$ to denote the real part of \mathbf{X} , $\text{diag}(\mathbf{x})$ to denote the diagonal matrix with its diagonal entries given by \mathbf{x} , $[\mathbf{X}]_{\mathcal{I},\mathcal{J}}$ to denote the submatrix of \mathbf{X} with the rows indexed by the set \mathcal{I} and columns indexed by the set \mathcal{J} , $a : b$ to denote the set $\{i | a \leq i \leq b, i \in \mathbb{Z}\}$ and \mathbf{I} to denote the identity matrix. We use $\mathcal{N}(\mathbf{x}; \boldsymbol{\mu}, \boldsymbol{\Sigma})$ and $\mathcal{CN}(\mathbf{x}; \boldsymbol{\mu}, \boldsymbol{\Sigma})$ to denote the real Gaussian distribution and the circularly-symmetric Gaussian distribution with mean vector $\boldsymbol{\mu}$ and covariance matrix $\boldsymbol{\Sigma}$. We use $\mathcal{M}(x; \mu, \kappa)$ to denote the Von Mises (VM) distribution with mean direction μ and concentration parameters κ . We use $\mathbb{E}[\cdot]$ to denote the expectation operator, \odot to denote the Hadamard product, \circ to denote the cross product, \otimes to denote the Kronecker product, $\|\cdot\|_p$ to denote the ℓ_p norm, and j to denote the imaginary unit.

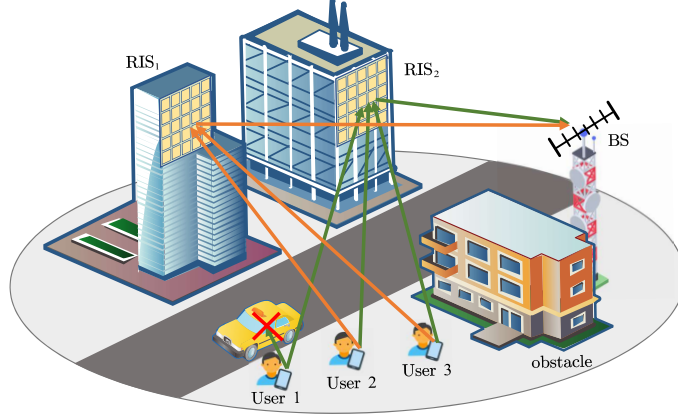


Fig. 1. System model.

II. SYSTEM MODEL

A. System Description

We consider a multi-RIS aided multiuser MIMO-OFDM system as illustrated in Fig. 1. In uplink transmission, a BS simultaneously receives the OFDM pilot signals transmitted by K single antenna users to achieve multiuser tracking. The LoS paths between BS and users are assumed to be obstructed by following [17], [23], [24], and the user signals are reflected by M RISs. We assume that the BS consists of N_B antennas arranged as a uniform linear array (ULA) and each RIS consists of $N_R = N_x \times N_y$ reflecting elements arranged as uniform planar array (UPA). The antenna/element interval is set to half of the carrier frequency wavelength λ . The BS simultaneously tracks the K users by estimating their positions in every pilot frame. Each pilot frame contains G OFDM symbols and each OFDM symbol occupied L subcarriers with bandwidth f_s . We assume a quasi-static flat fading channel model, where the channel coefficients and the user positions remain unchanged within a pilot frame.

Assume that a 3D Cartesian coordinate system has been set up appropriately. The positions of the BS, the m -th RIS and the k -th user in the t -th frame transmission are denoted by \mathbf{p}_B , $\mathbf{p}_{R,m}$ and $\mathbf{p}_k^{(t)}$ respectively. The positions of the BS and the RISs can be acquired by the user and the BS accurately in advance since the BS and the RISs are deployed stationarily.

B. Signal Model

We adopt the geometric channel model used in [17], [24]. In the t -th frame, the channel from the k -th user to the m -th RIS and from the m -th RIS to the BS over the l -th subcarrier are given

by

$$\mathbf{h}_{m,k}^{(t,l)} = \sqrt{\frac{\alpha}{1+\alpha}} \bar{\mathbf{h}}_{m,k}^{(t,l)} + \sqrt{\frac{1}{1+\alpha}} \tilde{\mathbf{h}}_{m,k}^{(t,l)}, \quad (1)$$

$$\mathbf{H}_m^{(t,l)} = \sqrt{\frac{\alpha}{1+\alpha}} \bar{\mathbf{H}}_m^{(l)} + \sqrt{\frac{1}{1+\alpha}} \tilde{\mathbf{H}}_m^{(t,l)}, \quad (2)$$

where $\tilde{\mathbf{h}}_{m,k}^{(t,l)}$ and $\tilde{\mathbf{H}}_m^{(t,l)}$ are the corresponding NLoS multi-path components; α is the Rician factor; $\bar{\mathbf{h}}_{m,k}^{(t,l)}$ and $\bar{\mathbf{H}}_m^{(l)}$ are the corresponding LoS path components given by

$$\bar{\mathbf{h}}_{m,k}^{(t,l)} = \zeta_{m,k}^{(t)} \rho_{m,k}^{(t)} e^{-j\frac{2\pi f_s l}{L} \tau_{m,k}^{(t)}} \mathbf{a}_R(\theta_{m,k,x}^{(t)}, \theta_{m,k,y}^{(t)}), \quad (3)$$

$$\bar{\mathbf{H}}_m^{(l)} = \rho_m e^{-j\frac{2\pi f_s l}{L} \tau_m} \mathbf{a}_B(\theta_m) \mathbf{a}_R^H(\phi_{m,x}, \phi_{m,y}), \quad (4)$$

where binary variable $\zeta_{m,k}^{(t)} \in \{0, 1\}$ indicates the existence of the LoS path between the m -th RIS and the k -th user; $\rho_{m,k}^{(t)}$ and $\tau_{m,k}^{(t)}$ denote the path gain and time delay of the LoS path between the k -th user and the m -th RIS in the t -th frame; ρ_m and τ_m denote the path gain and time delay of the LoS path between the m -th RIS and the BS; $\theta_{m,k,x}^{(t)}$ and $\theta_{m,k,y}^{(t)}$ denote the cosine of the AoA of the LoS path along the x direction and y direction of the m -th RIS w.r.t. the k -th user; $\phi_{m,x}$ and $\phi_{m,y}$ are the cosine of the AoD at the m -th RIS; θ_m is the cosine of AoA of the LoS path from the m -th RIS to BS; $\mathbf{a}_R(\cdot)$ and $\mathbf{a}_B(\cdot)$ are the steering vector of BS antennas and RIS elements, respectively, given by $\mathbf{a}_R(\theta_1, \theta_2) = \mathbf{a}_x(\theta_1) \otimes \mathbf{a}_y(\theta_2)$ and $\mathbf{a}_x(\theta) = [1, e^{j\pi\theta}, \dots, e^{j\pi\theta(N_x-1)}]^T$ for $x \in \{B, x, y\}$. We assume that the RIS PBF configuration remains the same for different subcarriers and varies over different OFDM symbols. Let $\boldsymbol{\omega}_m^{(t,g)} \in \mathbb{C}^{N_R}$ denotes the PBF vector of the m -th RIS in the g -th OFDM symbol. The received signal over the l -th subcarrier of the g -th OFDM symbol is given by

$$\mathbf{y}^{(t,g,l)} = \sum_{m=1}^M \sum_{k=1}^K \mathbf{H}_m^{(t,l)} \text{diag}(\boldsymbol{\omega}_m^{(t,g)}) \mathbf{h}_{m,k}^{(t,l)} x_k^{(t,l)} + \mathbf{w}^{(t,g,l)}, \quad (5)$$

where $x_k^{(t,l)}$ is the pilot signal of the k -th user and $\mathbf{w}^{(t,g,l)}$ is the additive white Gaussian noise. In user localization and tracking tasks, the information of user position $\mathbf{p}_k^{(t)}$ is contained in the channel parameters of the LoS path, i.e., $\theta_{m,k,x}^{(t)}$, $\theta_{m,k,y}^{(t)}$ and $\tau_{m,k}^{(t)}$. Therefore, we focus on the LoS path component and separate it from the NLoS multi-path components. With some manipulations, received signal (5) is simplified into a superposition of M steering vectors expressed as

$$\mathbf{y}^{(t,g,l)} = \sum_{m=1}^M [\mathbf{R}_m^{(t)}]_{g,l} \mathbf{a}_B(\theta_m) + \mathbf{n}^{(t,g,l)}. \quad (6)$$

Let $\mathbf{r}_{g,l}^{(t)} = \left[[\mathbf{R}_1^{(t)}]_{g,l}, \dots, [\mathbf{R}_M^{(t)}]_{g,l} \right]^T$ and $\mathbf{A}_B(\boldsymbol{\theta}) = [\mathbf{a}_B(\theta_1), \dots, \mathbf{a}_B(\theta_M)]$, a compact form of (6) is

$$\mathbf{y}^{(t,g,l)} = \mathbf{A}_B(\boldsymbol{\theta}) \mathbf{r}_{g,l}^{(t)} + \mathbf{n}^{(t,g,l)}, \quad (7)$$

where $\mathbf{n}^{(t,g,l)} \in \mathbb{C}^{N_B}$ is the interference-plus-noise term given by

$$\begin{aligned} \mathbf{n}^{(t,g,l)} = & \sum_{m=1}^M \sum_{k=1}^K \left(\tilde{\mathbf{H}}_m^{(t,l)} \text{diag}(\boldsymbol{\omega}_m^{(t,g)}) \tilde{\mathbf{h}}_{m,k}^{(t,l)} + \tilde{\mathbf{H}}_m^{(t,l)} \text{diag}(\boldsymbol{\omega}_m^{(t,g)}) \bar{\mathbf{h}}_{m,k}^{(t,l)} + \bar{\mathbf{H}}_m^{(l)} \text{diag}(\boldsymbol{\omega}_m^{(t,g)}) \tilde{\mathbf{h}}_{m,k}^{(t,l)} \right) x_k^{(t,l)} \\ & + \mathbf{w}^{(t,g,l)}. \end{aligned} \quad (8)$$

Due to the severe large-scale fading and reflection loss, the power of interference is generally 20 dB weaker than the LoS path [25]. We assume that the interference-plus-noise term follows complex Gaussian distribution [17], i.e., $\mathcal{CN}(\mathbf{n}^{(t,g,l)}; \mathbf{0}, \nu \mathbf{I})$. The complex amplitude $[\mathbf{R}_m^{(t)}]_{g,l}$ corresponding to the m -th RIS in (6) is given by

$$[\mathbf{R}_m^{(t)}]_{g,l} = \sum_{k=1}^K x_k^{(t,l)} \zeta_{m,k}^{(t)} \varrho_{m,k}^{(t)} e^{-j \frac{2\pi f_s l}{L} \zeta_{m,k}^{(t)}} (\boldsymbol{\omega}_m^{(t,g)})^T \mathbf{a}_R(\vartheta_{m,k,x}^{(t)}, \vartheta_{m,k,y}^{(t)}), \quad (9)$$

with $\varrho_{m,k}^{(t)} = \rho_{m,k} \rho_m$, $\vartheta_{m,k,x}^{(t)} = \theta_{m,k,x}^{(t)} - \phi_{m,x}$, $\vartheta_{m,k,y}^{(t)} = \theta_{m,k,y}^{(t)} - \phi_{m,y}$, and $\zeta_{m,k}^{(t)} = \tau_m + \tau_{m,k}^{(t)}$. We define $\mathbf{a}_L(\varsigma) = [1, e^{-j \frac{2\pi f_s}{L} \varsigma}, \dots, e^{-j \frac{2\pi f_s}{L} \varsigma(L-1)}]$. Let $\mathbf{W}_m^{(t)} = [\boldsymbol{\omega}_m^{(t,1)}, \dots, \boldsymbol{\omega}_m^{(t,G)}]$ and $\mathbf{x}_k^{(t)} = [x_k^{(t,1)}, \dots, x_k^{(t,L)}]^T$. The matrix $\mathbf{R}_m^{(t)} \in \mathbb{C}^{G \times L}$ is expressed by

$$\mathbf{R}_m^{(t)} = (\mathbf{W}_m^{(t)})^T \sum_{k=1}^K \zeta_{m,k}^{(t)} \varrho_{m,k}^{(t)} \mathbf{a}_R(\vartheta_{m,k,x}^{(t)}, \vartheta_{m,k,y}^{(t)}) (\mathbf{x}_k^{(t)} \odot \mathbf{a}_L(\zeta_{m,k}^{(t)}))^T. \quad (10)$$

From (10), we note that the channel parameters $\theta_{m,k,x}^{(t)}$, $\theta_{m,k,y}^{(t)}$ and $\tau_{m,k}^{(t)}$ are wrapped into the complex amplitude $\mathbf{R}_m^{(t)}$. The estimation of these channel parameters from $\mathbf{R}_m^{(t)}$ falls into the category of multidimensional line spectrum inference. The user position is further estimated based on the geometric constraints between $\zeta_{m,k}^{(t)}$, $\vartheta_{m,k,x}^{(t)}$ and $\vartheta_{m,k,y}^{(t)}$ and $\mathbf{p}_k^{(t)}$ given by

$$\vartheta_{m,k,x}^{(t)} = \frac{(\mathbf{p}_k^{(t)} - \mathbf{p}_{R,m})^T \mathbf{e}_{m,x}}{\|\mathbf{p}_k^{(t)} - \mathbf{p}_{R,m}\|_2} - \phi_{m,x}, \quad (11a)$$

$$\vartheta_{m,k,y}^{(t)} = \frac{(\mathbf{p}_k^{(t)} - \mathbf{p}_{R,m})^T \mathbf{e}_{m,y}}{\|\mathbf{p}_k^{(t)} - \mathbf{p}_{R,m}\|_2} - \phi_{m,y}, \quad (11b)$$

$$\zeta_{m,k}^{(t)} = \tau_m + \frac{\|\mathbf{p}_k^{(t)} - \mathbf{p}_{R,m}\|_2}{c_0}, \quad (11c)$$

where $\mathbf{e}_{m,x}$ and $\mathbf{e}_{m,y}$ are the x-axis and y-axis unit vectors of the m -th RIS, respectively, and c_0 denotes the speed of light.

C. Probabilistic Problem Formulation

We build a probability model for $\mathbf{p}_k^{(t)}$, $\vartheta_{m,k,x}^{(t)}$, $\vartheta_{m,k,y}^{(t)}$, $\varsigma_{m,k}^{(t)}$, $\zeta_{m,k}^{(t)}$, $\varrho_{m,k}^{(t)}$ and $\mathbf{y}^{(t,g,l)}$ in the whole tracking duration. Given the geometric constraint in (10), the conditional probability density functions (pdf) $p(\vartheta_{m,k,x}^{(t)}|\mathbf{p}_k^{(t)})$, $p(\vartheta_{m,k,y}^{(t)}|\mathbf{p}_k^{(t)})$ and $p(\varsigma_{m,k}^{(t)}|\mathbf{p}_k^{(t)})$ are given by

$$p(\vartheta_{m,k,x}^{(t)}|\mathbf{p}_k^{(t)}) = \delta \left(\vartheta_{m,k,x}^{(t)} - \frac{(\mathbf{p}_k^{(t)} - \mathbf{p}_{R,m})^T \mathbf{e}_{m,x}}{\|\mathbf{p}_k^{(t)} - \mathbf{p}_{R,m}\|_2} + \phi_{m,x} \right), \quad (12a)$$

$$p(\vartheta_{m,k,y}^{(t)}|\mathbf{p}_k^{(t)}) = \delta \left(\vartheta_{m,k,y}^{(t)} - \frac{(\mathbf{p}_k^{(t)} - \mathbf{p}_{R,m})^T \mathbf{e}_{m,y}}{\|\mathbf{p}_k^{(t)} - \mathbf{p}_{R,m}\|_2} + \phi_{m,y} \right), \quad (12b)$$

$$p(\varsigma_{m,k}^{(t)}|\mathbf{p}_k^{(t)}) = \delta \left(\varsigma_{m,k}^{(t)} - \frac{\|\mathbf{p}_k^{(t)} - \mathbf{p}_{R,m}\|_2}{c_0} - \tau_m \right), \quad (12c)$$

where $\delta(\cdot)$ is a Dirac delta function. The existence of the LoS paths between RISs and users may change over time due to the blockage of obstacles. The prior distribution of the cascaded channel path gain $\varrho_{m,k}^{(t)}$ is modeled by a complex Gaussian distribution, i.e., $p(\varrho_{m,k}^{(t)}) = \mathcal{CN}(\varrho_{m,k}^{(t)}; 0, \sigma_m^2)$. $\varrho_{m,k}^{(t)}$ is independent with $\varrho_{m',k'}^{(t')}$ for any $m \neq m'$, $k \neq k'$, $t \neq t'$. Given the observation model in (6), the likelihood function is represented by

$$p(\mathbf{y}^{(t,g,l)}|\{\vartheta_{m,x}^{(t)}, \vartheta_{m,y}^{(t)}, \varsigma_m^{(t)}, \zeta_m^{(t)}, \varrho_m^{(t)}\}_{m=1}^M) = p(\mathbf{y}^{(t,g,l)}|\mathbf{r}_{g,l}^{(t)}) \prod_{m=1}^M p([\mathbf{r}_{g,l}^{(t)}]_m|\vartheta_{m,x}^{(t)}, \vartheta_{m,y}^{(t)}, \varsigma_m^{(t)}, \zeta_m^{(t)}, \varrho_m^{(t)}), \quad (13)$$

where $\varrho_m^{(t)} = [\varrho_{m,1}^{(t)}, \dots, \varrho_{m,k}^{(t)}]^T$ and similar notations are applied to $\vartheta_{m,k,x}^{(t)}$, $\vartheta_{m,k,y}^{(t)}$, $\varsigma_{m,k}^{(t)}$ and $\zeta_{m,k}^{(t)}$. $p([\mathbf{r}_{g,l}^{(t)}]_m|\vartheta_{m,x}^{(t)}, \vartheta_{m,y}^{(t)}, \varsigma_m^{(t)}, \zeta_m^{(t)}, \varrho_m^{(t)})$ is a Dirac delta function derived from (9) and $p(\mathbf{y}^{(t,g,l)}|\mathbf{r}_{g,l}^{(t)}) = \mathcal{CN}(\mathbf{y}^{(t,g,l)}; \mathbf{A}_B(\boldsymbol{\theta}_k)\mathbf{r}_{g,l}^{(t)}, \nu\mathbf{I})$.

Considering the temporal correlation of user positions, we build a Markov transition probability model to characterize user movements. The difference of a user position between any two adjacent frames is modeled as an independent Gaussian noise [21]. The conditional probability of $\mathbf{p}_k^{(t)}$ given $\mathbf{p}_k^{(t-1)}$ is given by

$$p(\mathbf{p}_k^{(t)}|\mathbf{p}_k^{(t-1)}) = \mathcal{N}(\mathbf{p}_k^{(t)}; \mathbf{p}_k^{(t-1)}, \mathbf{C}_k) \quad (14)$$

with $\mathbf{C}_k = \text{diag}([\sigma_{k,x}^2, \sigma_{k,y}^2, \sigma_{k,z}^2]^T)$.

In the tracking duration, the binary variable $\zeta_{m,k}^{(t)}$ does not change frequently among different frames since the user continuously moves and the time gap of adjacent frames is small. The existence of the LoS path is correlated over time. Therefore, we use a birth and death process to model the state transition of $\zeta_{m,k}^{(t)}$, i.e.,

$$p(\zeta_{m,k}^{(t)} | \zeta_{m,k}^{(t-1)}) = \begin{cases} \left(1 - p_{l,m,k}^{(t)}\right)^{1-\zeta_{m,k}^{(t)}} \left(p_{l,m,k}^{(t)}\right)^{\zeta_{m,k}^{(t)}}, & \zeta_{m,k}^{(t-1)} = 0; \\ \left(p_{d,m,k}^{(t)}\right)^{1-\zeta_{m,k}^{(t)}} \left(1 - p_{d,m,k}^{(t)}\right)^{\zeta_{m,k}^{(t)}}, & \zeta_{m,k}^{(t-1)} = 1, \end{cases} \quad (15)$$

where $p_{l,m,k}^{(t)} = p(\zeta_{m,k}^{(t)} = 1 | \zeta_{m,k}^{(t-1)} = 0)$ and $p_{d,m,k}^{(t)} = p(\zeta_{m,k}^{(t)} = 0 | \zeta_{m,k}^{(t-1)} = 1)$. Then, the joint pdf of the random variables in each frame is given by

$$\begin{aligned} & p(\{\mathbf{p}_k^{(t)}\}, \{\zeta_{m,k}^{(t)}\}, \{\vartheta_{m,k,x}^{(t)}\}, \{\vartheta_{m,k,y}^{(t)}\}, \{\varsigma_{m,k}^{(t)}\}, \{\varrho_{m,k}^{(t)}\}, \{\mathbf{y}^{(t,g,l)}\}) \\ &= f_m(\{\mathbf{p}_k^{(t)}\}, \{\zeta_{m,k}^{(t)}\}) f_g(\{\vartheta_{m,k,x}^{(t)}\}, \{\vartheta_{m,k,y}^{(t)}\}, \{\varsigma_{m,k}^{(t)}\}, \{\varrho_{m,k}^{(t)}\} | \{\mathbf{p}_k^{(t)}\}) \\ & \quad \times f_l(\{\mathbf{y}^{(t,g,l)}\} | \{\vartheta_{m,k,x}^{(t)}\}, \{\vartheta_{m,k,y}^{(t)}\}, \{\varsigma_{m,k}^{(t)}\}, \{\varrho_{m,k}^{(t)}\}), \end{aligned} \quad (16)$$

where $\{x\}$ represents the collection of variable x over all considered indexes. Factors f_m , f_g and f_l are respectively given by

$$f_m(\cdot) = \prod_{k=1}^K \left(p(\mathbf{p}_k^{(0)}) \prod_{m=1}^M p(\zeta_{m,k}^{(0)}) \prod_{j=1}^t \left(p(\mathbf{p}_k^{(j)} | \mathbf{p}_k^{(j-1)}) p(\zeta_{m,k}^{(j)} | \zeta_{m,k}^{(j-1)}) \right) \right), \quad (17a)$$

$$f_g(\cdot) = \prod_{j=1}^t \prod_{m=1}^M \prod_{k=1}^K p(\vartheta_{m,k,x}^{(j)} | \mathbf{p}_k^{(j)}) p(\vartheta_{m,k,y}^{(j)} | \mathbf{p}_k^{(j)}) p(\varsigma_{m,k}^{(j)} | \mathbf{p}_k^{(j)}) p(\varrho_{m,k}^{(j)}), \quad (17b)$$

$$f_l(\cdot) = \prod_{j=1}^t \prod_{g=1}^G \prod_{l=1}^L p(\mathbf{y}^{(t,g,l)} | \{\vartheta_{m,x}^{(t)}, \vartheta_{m,y}^{(t)}, \varsigma_m^{(t)}, \zeta_m^{(t)}, \varrho_m^{(t)}\}_{m=1}^M), \quad (17c)$$

where $p(\mathbf{p}_k^{(0)})$ and $p(\zeta_{m,k}^{(0)})$ are respectively the distribution of $\mathbf{p}_k^{(t)}$ and $\zeta_{m,k}^{(t)}$ at the initial frame. In the multiuser tracking task, we aim to develop an online algorithm that in each frame the BS can estimate the position of each user $\mathbf{p}_k^{(t)}$ and the binary variable $\zeta_{m,k}^{(0)}$ given the historically received signal and the initial distribution. Despite the traditional minimum mean-square error (MMSE) and maximum *a posteriori* (MAP) estimators being desirable, the high computational complexity of the high dimension integral or the high dimensional search makes them intractable. In this paper, we provide a low-complexity approximate solution by following the message passing

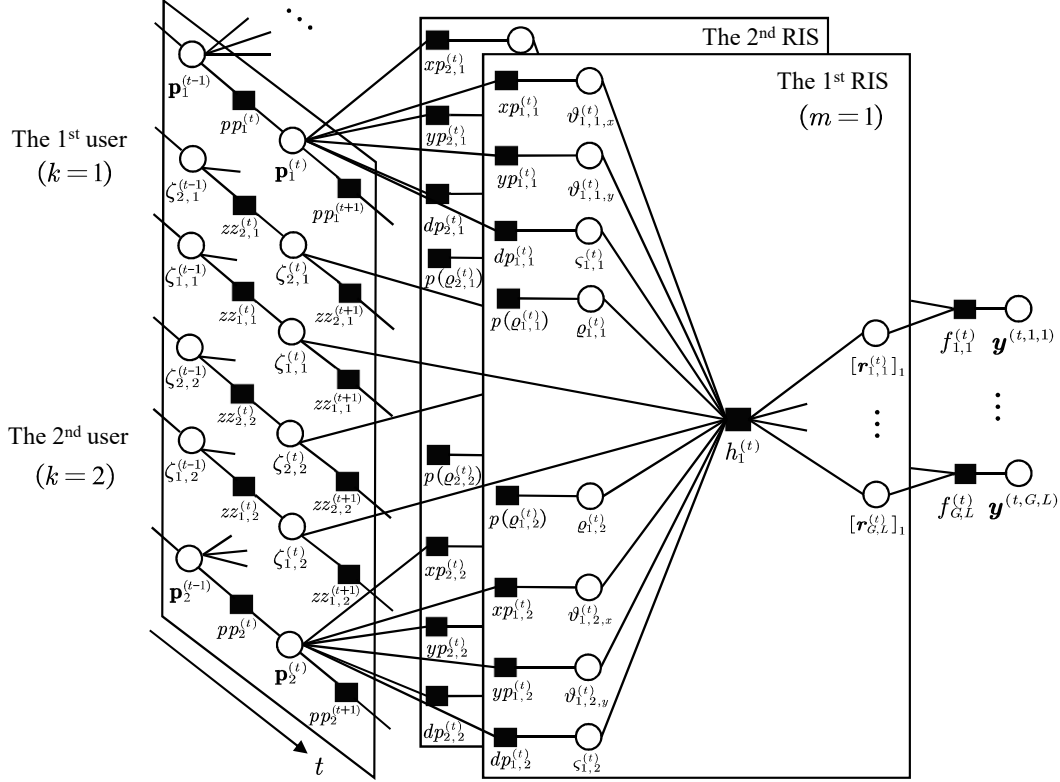


Fig. 2. Factor graph representation for $M = 2$ and $K = 2$, where we only depict the detail at the t -th frame for brevity.

principle and the variational Bayesian principle.

III. BAYESIAN MULTIUSER TRACKING ALGORITHM

The factor graph representation of the joint pdf (16) is shown in Fig. 2. We use blank circles to represent the variable nodes and black rectangles to represent factor nodes. The factor function of each factor node is listed in Table I. Denote by $\Delta_{a \rightarrow b}(\cdot)$ the message from node a to b , and by $\Delta_a(\cdot)$ the marginal message at variable node a . The mean vector and the covariance matrix of message $\Delta_{a \rightarrow b}(\cdot)$ are represented by $\mathbf{m}_{a \rightarrow b}$ and $\mathbf{C}_{a \rightarrow b}$. We perform sum-product message passing on the factor graph to estimate user positions in an online fashion.

A. Calculation of Messages $\Delta_{[\mathbf{r}_{g,l}^{(t)}]_m \rightarrow h_m^{(t)}}([\mathbf{r}_{g,l}^{(t)}]_m)$

The message passing from variable node $[\mathbf{r}_{g,l}^{(t)}]_m$ to factor node $h_m^{(t)}$ is calculated by

$$\Delta_{[\mathbf{r}_{g,l}^{(t)}]_m \rightarrow h_m^{(t)}}([\mathbf{r}_{g,l}^{(t)}]_m) \propto \frac{\int_{[\mathbf{r}_{g,l}^{(t)}]_m} \prod_{i=1}^M \Delta_{h_i^{(t)} \rightarrow [\mathbf{r}_{g,l}^{(t)}]_i}([\mathbf{r}_{g,l}^{(t)}]_i) p(\mathbf{y}^{(t,g,l)} | \mathbf{r}_{g,l}^{(t)})}{\Delta_{h_m^{(t)} \rightarrow [\mathbf{r}_{g,l}^{(t)}]_m}([\mathbf{r}_{g,l}^{(t)}]_m)}, \quad (18)$$

TABLE I
FACTOR NODES IN FIG. 2.

Factor Node	Factor Function
$pp_k^{(t)}$	$p(\mathbf{p}_k^{(t)} \mathbf{p}_k^{(t-1)}) = \mathcal{N}(\mathbf{p}_k^{(t)}; \mathbf{p}_k^{(t-1)}, \mathbf{C}_k)$
$xp_{m,k}^{(t)}$	$p(\vartheta_{m,k,x}^{(t)} \mathbf{p}_k^{(t)}) = \delta(\vartheta_{m,k,x}^{(t)} - \frac{(\mathbf{p}_k^{(t)} - \mathbf{p}_{R,m})^T \mathbf{e}_{m,x}}{\ \mathbf{p}_k^{(t)} - \mathbf{p}_{R,m}\ _2} + \phi_{m,x})$
$yp_{m,k}^{(t)}$	$p(\vartheta_{m,k,y}^{(t)} \mathbf{p}_k^{(t)}) = \delta(\vartheta_{m,k,y}^{(t)} - \frac{(\mathbf{p}_k^{(t)} - \mathbf{p}_{R,m})^T \mathbf{e}_{m,y}}{\ \mathbf{p}_k^{(t)} - \mathbf{p}_{R,m}\ _2} + \phi_{m,y})$
$dp_{m,k}^{(t)}$	$p(\zeta_{m,k}^{(t)} \mathbf{p}_k^{(t)}) = \delta(\zeta_{m,k}^{(t)} - \frac{\ \mathbf{p}_k^{(t)} - \mathbf{p}_{R,m}\ _2}{c_0} - \tau_m)$
$zz_{m,k}^{(t)}$	$p(\zeta_{m,k}^{(t)} \zeta_{m,k}^{(t-1)}) = \begin{cases} \left(1 - p_{l,m,k}^{(t)}\right)^{1-\zeta_{m,k}^{(t)}} \left(p_{l,m,k}^{(t)}\right)^{\zeta_{m,k}^{(t)}}, & \zeta_{m,k}^{(t-1)} = 0 \\ \left(p_{d,m,k}^{(t)}\right)^{1-\zeta_{m,k}^{(t)}} \left(1 - p_{d,m,k}^{(t)}\right)^{\zeta_{m,k}^{(t)}}, & \zeta_{m,k}^{(t-1)} = 1 \end{cases}$
$p(\varrho_{m,k}^{(t)})$	$\mathcal{CN}(\varrho_{m,k}^{(t)}; 0, \sigma_m^{(t)})$
$h_m^{(t)}$	$\prod_{g=1}^G \prod_{l=1}^L p([\mathbf{r}_{g,l}^{(t)}]_m \vartheta_{m,x}^{(t)}, \vartheta_{m,y}^{(t)}, \zeta_m^{(t)}, \zeta_m^{(t)}, \varrho_m^{(t)}) = \prod_{g=1}^G \prod_{l=1}^L \delta([\mathbf{r}_{g,l}^{(t)}]_m - [\mathbf{R}_m^{(t)}]_{g,l})$
$f_{g,l}^{(t)}$	$p(\mathbf{y}^{(t,g,l)} \mathbf{r}_{g,l}^{(t)}) = \mathcal{CN}(\mathbf{y}^{(t,g,l)}; \mathbf{A}_B(\boldsymbol{\theta}_k) \mathbf{r}_{g,l}^{(t)}, \nu \mathbf{I})$

where $\int_{\setminus [\mathbf{r}_{g,l}^{(t)}]_m}$ denotes the integral over all involved variables except $[\mathbf{r}_{g,l}^{(t)}]_m$. In practice, the BS is generally equipped with large-scale antennas, and the RISs are separately deployed with different θ_m . Therefore, the columns of $\mathbf{A}_B(\boldsymbol{\theta})$ are approximately orthogonal. Based on the central limit theorem [26], the message $\Delta_{h_m^{(t)} \rightarrow [\mathbf{r}_{g,l}^{(t)}]_m}([\mathbf{r}_{g,l}^{(t)}]_m)$ is approximated as a Gaussian message. Given the linear model in (7), the message $\Delta_{[\mathbf{r}_{g,l}^{(t)}]_m \rightarrow h_m^{(t)}}([\mathbf{r}_{g,l}^{(t)}]_m)$ is approximately calculated by

$$\Delta_{[\mathbf{r}_{g,l}^{(t)}]_m \rightarrow h_m^{(t)}}([\mathbf{r}_{g,l}^{(t)}]_m) = \mathcal{CN}\left([\mathbf{r}_{g,l}^{(t)}]_m; \frac{\mathbf{a}_B^H(\theta_i) \mathbf{y}^{(t,g,l)}}{N_B}, \frac{\nu}{N_B}\right). \quad (19)$$

B. Messages Approximated by Variational Inference

For $\forall t, 1 \leq k \leq K, 1 \leq m \leq M$, the messages from variable node $\vartheta_{m,k,x}^{(t)}$ to factor node $xp_{m,k}^{(t)}$ are calculated by

$$\Delta_{\vartheta_{m,k,x}^{(t)} \rightarrow xp_{m,k}^{(t)}}(\vartheta_{m,k,x}^{(t)}) \propto \frac{\Delta_{\vartheta_{m,k,x}^{(t)}}(\vartheta_{m,k,x}^{(t)})}{\Delta_{xp_{m,k}^{(t)} \rightarrow \vartheta_{m,k,x}^{(t)}}(\vartheta_{m,k,x}^{(t)})}, \quad (20)$$

where $\Delta_{xp_{m,k}^{(t)} \rightarrow \vartheta_{m,k,x}^{(t)}}(\vartheta_{m,k,x}^{(t)})$ is calculated by

$$\Delta_{xp_{m,k}^{(t)} \rightarrow \vartheta_{m,k,x}^{(t)}}(\vartheta_{m,k,x}^{(t)}) \propto \int_{\mathbf{p}_k^{(t)}} \Delta_{pp_k^{(t)} \rightarrow \mathbf{p}_k^{(t)}}(\mathbf{p}_k^{(t)}) p(\vartheta_{m,k,x}^{(t)} | \mathbf{p}_k^{(t)}) \quad (21)$$

The messages passing from factor nodes $xp_{m,k}^{(t)}$, $xp_{m,k}^{(t)}$, and $xp_{m,k}^{(t)}$ to variable node $\mathbf{p}_k^{(t)}$ are omitted in (21). Given the Gaussian message $\Delta_{pp_k^{(t)} \rightarrow \mathbf{p}_k^{(t)}}(\mathbf{p}_k^{(t)})$ derived in Section III-C, $\Delta_{xp_{m,k}^{(t)} \rightarrow \vartheta_{m,k,x}^{(t)}}(\vartheta_{m,k,x}^{(t)})$

is well approximated by a VM distribution $\mathcal{M}(\vartheta_{m,k,x}^{(t)}; \mu_{xp_{m,k}^{(t)} \rightarrow \vartheta_{m,k,x}^{(t)}}, \kappa_{xp_{m,k}^{(t)} \rightarrow \vartheta_{m,k,x}^{(t)}})$ where [21]

$$\mu_{xp_{m,k}^{(t)} \rightarrow \vartheta_{m,k,x}^{(t)}} = \frac{(\mathbf{m}_{pp_k^{(t)} \rightarrow \mathbf{p}_k^{(t)}} - \mathbf{p}_{R,m})^T \mathbf{e}_{m,x}}{\|\mathbf{m}_{pp_k^{(t)} \rightarrow \mathbf{p}_k^{(t)}} - \mathbf{p}_{R,m}\|_2} - \phi_{m,x}, \quad (22a)$$

$$\kappa_{xp_{m,k}^{(t)} \rightarrow \vartheta_{m,k,x}^{(t)}} = \frac{\|\mathbf{m}_{pp_k^{(t)} \rightarrow \mathbf{p}_k^{(t)}} - \mathbf{p}_{R,m}\|_2^6}{(1 - (\mu_{xp_{m,k}^{(t)} \rightarrow \vartheta_{m,k,x}^{(t)}} + \phi_{m,x})^2) \mathbf{q}_{m,k}^{(t)T} \mathbf{C}_{pp_k^{(t)} \rightarrow \mathbf{p}_k^{(t)}} \mathbf{q}_{m,k}^{(t)}}, \quad (22b)$$

with $\mathbf{q}_{m,k}^{(t)} = ((\mathbf{m}_{pp_k^{(t)} \rightarrow \mathbf{p}_k^{(t)}} - \mathbf{p}_{R,m}) \circ \mathbf{e}_{m,x}) \circ (\mathbf{m}_{pp_k^{(t)} \rightarrow \mathbf{p}_k^{(t)}} - \mathbf{p}_{R,m})$. Messages $\Delta_{\vartheta_{m,k,y}^{(t)} \rightarrow yp_{m,k}^{(t)}}(\vartheta_{m,k,y}^{(t)})$

and $\Delta_{\varsigma_{m,k}^{(t)} \rightarrow dp_{m,k}^{(t)}}(\varsigma_{m,k}^{(t)})$ are calculated similarly by $\Delta_{\vartheta_{m,k,y}^{(t)} \rightarrow yp_{m,k}^{(t)}}(\vartheta_{m,k,y}^{(t)}) \propto \frac{\Delta_{\vartheta_{m,k,y}^{(t)}}(\vartheta_{m,k,y}^{(t)})}{\Delta_{yp_{m,k}^{(t)} \rightarrow \vartheta_{m,k,y}^{(t)}}(\vartheta_{m,k,y}^{(t)})}$

and $\Delta_{\varsigma_{m,k}^{(t)} \rightarrow dp_{m,k}^{(t)}}(\varsigma_{m,k}^{(t)}) \propto \frac{\Delta_{\varsigma_{m,k}^{(t)}}(\varsigma_{m,k}^{(t)})}{\Delta_{dp_{m,k}^{(t)} \rightarrow \varsigma_{m,k}^{(t)}}(\varsigma_{m,k}^{(t)})}$ with $\Delta_{yp_{m,k}^{(t)} \rightarrow \vartheta_{m,k,y}^{(t)}}(\vartheta_{m,k,y}^{(t)})$ and $\Delta_{dp_{m,k}^{(t)} \rightarrow \varsigma_{m,k}^{(t)}}(\varsigma_{m,k}^{(t)})$ are

respectively approximated by VM distributions as $\mathcal{M}(\vartheta_{m,k,y}^{(t)}; \mu_{yp_{m,k}^{(t)} \rightarrow \vartheta_{m,k,y}^{(t)}}, \kappa_{yp_{m,k}^{(t)} \rightarrow \vartheta_{m,k,y}^{(t)}})$ and $\mathcal{M}(\varsigma_{m,k}^{(t)}; \mu_{dp_{m,k}^{(t)} \rightarrow \varsigma_{m,k}^{(t)}}, \kappa_{dp_{m,k}^{(t)} \rightarrow \varsigma_{m,k}^{(t)}})$. Due to the complex form of factor nodes $\{h_m^{(t)}\}$, it is difficult

to perform the sum-product rule on these nodes. Inspired by the variational inference of line spectra [27], [28], in the following, we adopt the variational inference approach to obtain the approximation of $\Delta_{\vartheta_{m,k,x}^{(t)}}(\vartheta_{m,k,x}^{(t)})$, $\Delta_{\vartheta_{m,k,y}^{(t)}}(\vartheta_{m,k,y}^{(t)})$, $\Delta_{\varsigma_{m,k}^{(t)}}(\varsigma_{m,k}^{(t)})$, $\Delta_{\varrho_{m,k}^{(t)}}(\varrho_{m,k}^{(t)})$, and $\Delta_{\varsigma_{m,k}^{(t)}}(\varsigma_{m,k}^{(t)})$. Note that the algorithms in [27], [28] are not applicable due to the existence of $\mathbf{W}_m^{(t)}$ in (10).

Our derivation extends the variational inference of line spectra to a more general form. The variational inference is parallelly performed over each RIS for each frame. For notation brevity, we omit indexes t and m in the derivation.

Defining

$$\begin{aligned} \Delta(\boldsymbol{\vartheta}_x, \boldsymbol{\vartheta}_y, \boldsymbol{\varsigma}, \boldsymbol{\zeta}, \boldsymbol{\varrho}) &= \prod_{k=1}^K \Delta_{xp_k \rightarrow \vartheta_{k,x}}(\vartheta_{k,x}) \Delta_{yp_k \rightarrow \vartheta_{k,y}}(\vartheta_{k,y}) \Delta_{dp_k \rightarrow \varsigma_k}(\varsigma_k) \Delta_{zz_k \rightarrow \zeta_k}(\zeta_k) p(\varrho_k) \\ &\times \int_{\mathbf{R}} \prod_{g=1}^G \prod_{l=1}^L p(r_{g,l} | \boldsymbol{\vartheta}_x, \boldsymbol{\vartheta}_y, \boldsymbol{\varsigma}_k, \boldsymbol{\zeta}_k, \boldsymbol{\varrho}) \Delta_{r_{g,l} \rightarrow h}(r_{g,l}), \end{aligned} \quad (23)$$

the basic idea of variational inference is to find the surrogate pdf $q(\boldsymbol{\vartheta}_x, \boldsymbol{\vartheta}_y, \boldsymbol{\varsigma}, \boldsymbol{\zeta}, \boldsymbol{\varrho})$ that minimizes the Kullback-Leibler (KL) divergence between the surrogate pdf and the objective pdf $\Delta(\boldsymbol{\vartheta}_x, \boldsymbol{\vartheta}_y, \boldsymbol{\varsigma}, \boldsymbol{\zeta}, \boldsymbol{\varrho})$, which is equivalent to maximizing the evidence lower bound [29]

$$\mathcal{L}(q(\boldsymbol{\vartheta}_x, \boldsymbol{\vartheta}_y, \boldsymbol{\varsigma}, \boldsymbol{\zeta}, \boldsymbol{\varrho})) = \mathbb{E}_{q(\boldsymbol{\vartheta}_x, \boldsymbol{\vartheta}_y, \boldsymbol{\varsigma}, \boldsymbol{\zeta}, \boldsymbol{\varrho})} \left[\ln \frac{\Delta(\boldsymbol{\vartheta}_x, \boldsymbol{\vartheta}_y, \boldsymbol{\varsigma}, \boldsymbol{\zeta}, \boldsymbol{\varrho})}{q(\boldsymbol{\vartheta}_x, \boldsymbol{\vartheta}_y, \boldsymbol{\varsigma}, \boldsymbol{\zeta}, \boldsymbol{\varrho})} \right]. \quad (24)$$

Assume that the surrogate pdf admits a factorization as

$$q(\boldsymbol{\vartheta}_x, \boldsymbol{\vartheta}_y, \boldsymbol{\varsigma}, \boldsymbol{\zeta}, \boldsymbol{\varrho}) = q(\boldsymbol{\zeta})q(\boldsymbol{\varrho}) \prod_{k=1}^K q(\vartheta_{k,x})q(\vartheta_{k,y})q(\varsigma_k), \quad (25)$$

where $q(\boldsymbol{\zeta})$ is restricted to satisfy $q(\boldsymbol{\zeta}) = \delta(\boldsymbol{\zeta} - \hat{\boldsymbol{\zeta}})$. Given the factor $q(\vartheta_{k,x})$, $q(\vartheta_{k,y})$ and $q(\varsigma_k)$, we obtain the estimations of random variables $\hat{\vartheta}_{k,x} = \arg(\mathbb{E}_{q(\vartheta_{k,x})}[e^{\mathcal{I}\vartheta_{k,x}}])$, $\hat{\vartheta}_{k,y} = \arg(\mathbb{E}_{q(\vartheta_{k,y})}[e^{\mathcal{I}\vartheta_{k,y}}])$ and $\hat{\varsigma}_k = \arg(\mathbb{E}_{q(\varsigma_k)}[e^{\mathcal{I}\varsigma_k}])$, and the estimations of steering vectors $\hat{\mathbf{a}}_x(\vartheta_{k,x}) = \mathbb{E}_{q(\vartheta_{k,x})}[\mathbf{a}_x(\vartheta_{k,x})]$, $\hat{\mathbf{a}}_y(\vartheta_{k,y}) = \mathbb{E}_{q(\vartheta_{k,y})}[\mathbf{a}_y(\vartheta_{k,y})]$, and $\hat{\mathbf{a}}_L(\varsigma_k) = \mathbb{E}_{q(\varsigma_k)}[\mathbf{a}_L(\varsigma_k)]$. Given the factor $q(\boldsymbol{\varrho})$, we obtain $\hat{\boldsymbol{\varrho}} = \mathbb{E}_{q(\boldsymbol{\varrho})}[\boldsymbol{\varrho}]$ and $\hat{\mathbf{C}}_{\boldsymbol{\varrho}} = \mathbb{E}_{q(\boldsymbol{\varrho})}[\boldsymbol{\varrho}\boldsymbol{\varrho}^H] - \hat{\boldsymbol{\varrho}}\hat{\boldsymbol{\varrho}}^H$. Given the factor $q(\boldsymbol{\zeta})$, the support set of the non-zero components in $\boldsymbol{\zeta}$ is estimated by $\hat{\mathcal{S}} = \{j | 1 \leq j \leq K, \hat{\zeta}_j = 1\}$. As maximizing \mathcal{L} over all the factors simultaneously is intractable, we adopt alternating optimization and maximize \mathcal{L} over each factor independently with the other factors keeping invariant. The factors are iteratively updated until converge. We present the details of the inference in the following.

1) *Calculate $q(\vartheta_{k,x})$ and $q(\vartheta_{k,y})$:* As derived in Appendix A, for $k \in \hat{\mathcal{S}}$, maximizing \mathcal{L} w.r.t. $q(\vartheta_{k,x})$ gives

$$\ln q(\vartheta_{k,x}) = \ln \Delta_{xp_k \rightarrow \vartheta_{k,x}}(\vartheta_{k,x}) + \text{Re}\{\boldsymbol{\beta}_k^H \mathbf{a}_x(\vartheta_{k,x}) \otimes \hat{\mathbf{a}}_y(\vartheta_{k,y})\} - \chi_k \mathbb{E}_{q(\vartheta_{k,y})} \left[\left\| \mathbf{W}^T \mathbf{a}_R(\vartheta_{k,x}, \vartheta_{k,y}) \right\|_2^2 \right]. \quad (26)$$

The calculation of $\mathbb{E}_{q(\vartheta_{k,y})} \left[\left\| \mathbf{W}^T \mathbf{a}_R(\vartheta_{k,x}, \vartheta_{k,y}) \right\|_2^2 \right]$ can be found in Appendix B; $\boldsymbol{\beta}_k$ and χ_k are given by

$$\boldsymbol{\beta}_k = \frac{2N_B}{\nu} \mathbf{W}^* \left(\hat{\varrho}_k^* \mathbf{R} - \mathbf{W}^T \sum_{j \in \mathcal{S} \setminus k} ([\hat{\mathbf{C}}_{\boldsymbol{\varrho}}]_{j,k} + \hat{\varrho}_j \hat{\varrho}_k^*) \hat{\mathbf{a}}_R(\vartheta_{j,x}, \vartheta_{j,y}) \mathbf{x}_j^T \odot \hat{\mathbf{a}}_L^T(\varsigma_j) \right) \mathbf{x}_k^* \odot \hat{\mathbf{a}}_L^*(\varsigma_k) \quad (27a)$$

$$\chi_k = \frac{N_B}{\nu} ([\hat{\mathbf{C}}_{\boldsymbol{\varrho}}]_{k,k} + \hat{\varrho}_k \hat{\varrho}_k^*) \left\| \mathbf{x}_k \odot \hat{\mathbf{a}}_L(\varsigma_k) \right\|_2^2. \quad (27b)$$

For $k \notin \hat{\mathcal{S}}$, we have $\ln q(\vartheta_{k,x}) = \ln \Delta_{xp_k \rightarrow \vartheta_{k,x}}(\vartheta_{k,x})$. The posterior pdf $q(\vartheta_{k,x})$ in (26) is well approximated by a VM distribution $\mathcal{M}(\vartheta_{k,x}; \mu_{\vartheta_{k,x}}, \kappa_{\vartheta_{k,x}})$, where $\mu_{\vartheta_{k,x}}$ and $\kappa_{\vartheta_{k,x}}$ are set to be the maximum of $\ln q(\vartheta_{k,x})$ and $A^{-1}(\exp(\frac{1}{2(\ln q(\mu_{\vartheta_{k,x}}))''}))$ respectively. $A^{-1}(\cdot)$ is the inverse of function $A(\cdot) = I_1(\cdot)/I_0(\cdot)$ given in [30], where $I_i(\cdot)$ is the modified Bessel function of the first kind in order i . We resort to the *gradient descent method* (GDM) to find the local maximum of $\ln q(\vartheta_{k,x})$. The gradient descent search starts from the the mean of $\Delta_{xp_k \rightarrow \vartheta_{k,x}}(\vartheta_{k,x})$. Similarly, $q(\vartheta_{k,y})$ can be approximated by $\mathcal{M}(\vartheta_{k,y}; \mu_{\vartheta_{k,y}}, \kappa_{\vartheta_{k,y}})$.

2) *Calculate $q(\varsigma_k)$* : Similar to the calculation of $q(\vartheta_{k,x})$ and $q(\vartheta_{k,y})$, for $k \in \hat{\mathcal{S}}$, maximizing \mathcal{L} w.r.t. $q(\varsigma_k)$ gives

$$\ln q(\varsigma_k) = \ln \Delta_{dp_k \rightarrow \varsigma_k}(\varsigma_k) + \text{Re}\{\boldsymbol{\beta}_{\varsigma,k}^H \mathbf{a}_L(\varsigma_k)\} + \text{const}, \quad (28)$$

where $\boldsymbol{\beta}_{\varsigma,k}$ is given by

$$\boldsymbol{\beta}_{\varsigma,k} = \frac{2N_B}{\nu} \text{diag}(\mathbf{x}_k^*) \left(\hat{\boldsymbol{\rho}}_k^* \mathbf{R}^T - \sum_{j \in \hat{\mathcal{S}} \setminus k} ([\hat{\mathbf{C}}_{\boldsymbol{\rho}}]_{j,k} + \hat{\rho}_j \hat{\rho}_k^*) \mathbf{x}_j \odot \mathbf{a}_L(\varsigma_j) \mathbf{a}_R^T(\vartheta_{j,x}, \vartheta_{j,y}) \mathbf{W} \right) \mathbf{W}^H \hat{\mathbf{a}}_R^*(\vartheta_{k,x}, \vartheta_{k,y}). \quad (29)$$

For $k \notin \hat{\mathcal{S}}$, we have $\ln q(\varsigma_k) = \ln \Delta_{dp_k \rightarrow \varsigma_k}(\varsigma_k)$. The posterior pdf $q(\varsigma_k)$ can be approximated by a VM distribution $\mathcal{M}(\varsigma_k; \mu_{\varsigma_k}, \kappa_{\varsigma_k})$ using Algorithm 2 from [27].

3) *Calculate $q(\boldsymbol{\rho})$* : Maximizing \mathcal{L} w.r.t. $q(\boldsymbol{\rho})$ gives

$$q(\boldsymbol{\rho}) = \mathcal{CN}([\boldsymbol{\rho}]_{\hat{\mathcal{S}}}; [\hat{\boldsymbol{\rho}}]_{\hat{\mathcal{S}}}, [\hat{\mathbf{C}}_{\boldsymbol{\rho}}]_{\hat{\mathcal{S}}, \hat{\mathcal{S}}}) \prod_{l \notin \hat{\mathcal{S}}} \delta(\rho_l), \quad (30)$$

where $\hat{\boldsymbol{\rho}} = \frac{N_B}{\nu} \hat{\mathbf{C}}_{\boldsymbol{\rho}} \mathbf{h}$ and $\hat{\mathbf{C}}_{\boldsymbol{\rho}} = \left(\frac{N_B}{\nu} \mathbf{J} + \frac{1}{\sigma} \mathbf{I} \right)^{-1}$ with the entries of \mathbf{h} and \mathbf{J} given by

$$[\mathbf{h}]_j = \text{Tr}(\mathbf{x}_j^* \odot \hat{\mathbf{a}}_L^*(\varsigma_j) \hat{\mathbf{a}}_R^H(\vartheta_{j,x}, \vartheta_{j,y}) \mathbf{W}^* \mathbf{R}), \quad (31a)$$

$$[\mathbf{J}]_{i,j} = \begin{cases} \|\mathbf{x}_i \odot \hat{\mathbf{a}}_L(\varsigma_i)\|_2^2 \mathbb{E}_{q(\vartheta_{i,x})q(\vartheta_{i,y})} [\|\mathbf{W}^T \mathbf{a}_R(\vartheta_{i,x}, \vartheta_{i,y})\|_2^2], & i = j; \\ \mathbf{x}_j^T \odot \hat{\mathbf{a}}_L^T(\varsigma_j) \mathbf{x}_i^* \odot \hat{\mathbf{a}}_L^*(\varsigma_i) \hat{\mathbf{a}}_R^H(\vartheta_{i,x}, \vartheta_{i,y}) \mathbf{W}^* \mathbf{W}^T \hat{\mathbf{a}}_R(\vartheta_{j,x}, \vartheta_{j,y}), & i \neq j. \end{cases} \quad (31b)$$

The calculation of $\mathbb{E}_{q(\vartheta_{i,x})q(\vartheta_{i,y})} [\|\mathbf{W}^T \mathbf{a}_R(\vartheta_{i,x}, \vartheta_{i,y})\|_2^2]$ can be found in Appendix B.

4) *Calculate $q(\boldsymbol{\zeta})$* : We calculate $q(\boldsymbol{\zeta})$ by plugging (25) into (24) and maximizing \mathcal{L} w.r.t. $q(\boldsymbol{\zeta})$. Since $q(\boldsymbol{\zeta}) = \delta(\boldsymbol{\zeta} - \hat{\boldsymbol{\zeta}})$, we obtain

$$\begin{aligned} \mathcal{L}(\hat{\boldsymbol{\zeta}}) &= \ln \det \left(\mathbf{J}_{\hat{\mathcal{S}}, \hat{\mathcal{S}}} + \frac{\nu}{N_B \sigma} \mathbf{I} \right)^{-1} + \frac{N_B}{\nu} \mathbf{h}_{\hat{\mathcal{S}}}^H \left(\mathbf{J}_{\hat{\mathcal{S}}, \hat{\mathcal{S}}} + \frac{\nu}{N_B \sigma} \mathbf{I} \right)^{-1} \mathbf{h}_{\hat{\mathcal{S}}} \\ &\quad + \|\boldsymbol{\zeta}\|_0 \ln \frac{\nu}{N_B \sigma} + \prod_{k=1}^K \Delta_{zz_k \rightarrow \varsigma_k}(\varsigma_k) + \text{const}. \end{aligned} \quad (32)$$

We adopt the greedy iterative search provided in [27] to find a local maximum of $\mathcal{L}(\hat{\boldsymbol{\zeta}})$. In the i -th iteration, K test variables $\{\hat{\boldsymbol{\zeta}}_k^i\}_{k=1}^K$ are generated by flip the k -th element of $\hat{\boldsymbol{\zeta}}^{i-1}$ for $k = 1, \dots, K$. $\hat{\boldsymbol{\zeta}}^i$ is obtained by calculating $\mathcal{L}(\hat{\boldsymbol{\zeta}}_k^i) - \mathcal{L}(\hat{\boldsymbol{\zeta}}^{i-1})$ for each $\hat{\boldsymbol{\zeta}}_k^i$ and find the largest non-negative term.

For $\forall t$ and $1 \leq m \leq M$, the factors $q(\vartheta_{m,k,x}^{(t)})$, $q(\vartheta_{m,k,y}^{(t)})$, and $q(\varsigma_{m,k}^{(t)})$ are first initialized by the message $\Delta_{xp_{m,k}^{(t)} \rightarrow \vartheta_{m,k,x}^{(t)}}(\vartheta_{m,k,x}^{(t)})$, $\Delta_{yp_{m,k}^{(t)} \rightarrow \vartheta_{m,k,y}^{(t)}}(\vartheta_{m,k,y}^{(t)})$, and $\Delta_{dp_{m,k}^{(t)} \rightarrow \varsigma_{m,k}^{(t)}}(\varsigma_{m,k}^{(t)})$. Factor $q(\vartheta_{m,k,x}^{(t)})$ and $q(\varsigma_{m,k}^{(t)})$ are then initialized by (30) and maximizing $\mathcal{L}(\hat{\varsigma}_m^{(t)})$ respectively. Since the family of VM distributions is closed under multiplication up to scaling, we calculate (20) and obtain the approximated message $\Delta_{\vartheta_{m,k,x}^{(t)} \rightarrow xp_{m,k}^{(t)}}(\vartheta_{m,k,x}^{(t)})$ as

$$\Delta_{\vartheta_{m,k,x}^{(t)} \rightarrow xp_{m,k}^{(t)}}(\vartheta_{m,k,x}^{(t)}) = \mathcal{M}(\vartheta_{m,k,x}^{(t)}; \mu_{\vartheta_{m,k,x}^{(t)} \rightarrow xp_{m,k}^{(t)}}^{(t)}, \kappa_{\vartheta_{m,k,x}^{(t)} \rightarrow xp_{m,k}^{(t)}}^{(t)}), \quad (33a)$$

where $\mu_{\vartheta_{m,k,x}^{(t)} \rightarrow xp_{m,k}^{(t)}}^{(t)}$ and $\kappa_{\vartheta_{m,k,x}^{(t)} \rightarrow xp_{m,k}^{(t)}}^{(t)}$ satisfy

$$\kappa_{\vartheta_{m,k,x}^{(t)} \rightarrow xp_{m,k}^{(t)}}^{(t)} \exp(j\mu_{\vartheta_{m,k,x}^{(t)} \rightarrow xp_{m,k}^{(t)}}^{(t)}) = \kappa_{\vartheta_{m,k,x}^{(t)}}^{(t)} \exp(j\mu_{\vartheta_{m,k,x}^{(t)}}^{(t)}) - \kappa_{xp_{m,k}^{(t)} \rightarrow \vartheta_{m,k,x}^{(t)}}^{(t)} \exp(j\mu_{xp_{m,k}^{(t)} \rightarrow \vartheta_{m,k,x}^{(t)}}^{(t)}).$$

Messages $\Delta_{\vartheta_{m,k,y}^{(t)} \rightarrow yp_{m,k}^{(t)}}(\vartheta_{m,k,y}^{(t)})$ and $\Delta_{\varsigma_{m,k}^{(t)} \rightarrow dp_{m,k}^{(t)}}(\varsigma_{m,k}^{(t)})$ are calculated similarly.

C. Calculation of Messages Passing Between Frames

1) Messages from $\mathbf{p}_k^{(t)}$ to $pp_k^{(t+1)}$: For $1 \leq k \leq K$,

$$\Delta_{\mathbf{p}_k^{(t)} \rightarrow pp_k^{(t+1)}}(\mathbf{p}_k^{(t)}) \propto \Delta_{pp_k^{(t)} \rightarrow \mathbf{p}_k^{(t)}}(\mathbf{p}_k^{(t)}) \prod_{m=1}^M \Delta_{xp_{m,k}^{(t)} \rightarrow \mathbf{p}_k^{(t)}}(\mathbf{p}_k^{(t)}) \Delta_{yp_{m,k}^{(t)} \rightarrow \mathbf{p}_k^{(t)}}(\mathbf{p}_k^{(t)}) \Delta_{dp_{m,k}^{(t)} \rightarrow \mathbf{p}_k^{(t)}}(\mathbf{p}_k^{(t)}) \quad (34)$$

where

$$\Delta_{xp_{m,k}^{(t)} \rightarrow \mathbf{p}_k^{(t)}}(\mathbf{p}_k^{(t)}) = \int_{\vartheta_{m,k,x}^{(t)}} \Delta_{\vartheta_{m,k,x}^{(t)} \rightarrow xp_{m,k}^{(t)}}(\vartheta_{m,k,x}^{(t)}) p(\vartheta_{m,k,x}^{(t)} | \mathbf{p}_k^{(t)}), \quad (35a)$$

$$\Delta_{yp_{m,k}^{(t)} \rightarrow \mathbf{p}_k^{(t)}}(\mathbf{p}_k^{(t)}) = \int_{\vartheta_{m,k,y}^{(t)}} \Delta_{\vartheta_{m,k,y}^{(t)} \rightarrow yp_{m,k}^{(t)}}(\vartheta_{m,k,y}^{(t)}) p(\vartheta_{m,k,y}^{(t)} | \mathbf{p}_k^{(t)}), \quad (35b)$$

$$\Delta_{dp_{m,k}^{(t)} \rightarrow \mathbf{p}_k^{(t)}}(\mathbf{p}_k^{(t)}) = \int_{\varsigma_{m,k}^{(t)}} \Delta_{\varsigma_{m,k}^{(t)} \rightarrow dp_{m,k}^{(t)}}(\varsigma_{m,k}^{(t)}) p(\varsigma_{m,k}^{(t)} | \mathbf{p}_k^{(t)}). \quad (35c)$$

As derived in Appendix C, the product of messages $\Delta_{xp_{m,k}^{(t)} \rightarrow \mathbf{p}_k^{(t)}}(\mathbf{p}_k^{(t)})$, $\Delta_{yp_{m,k}^{(t)} \rightarrow \mathbf{p}_k^{(t)}}(\mathbf{p}_k^{(t)})$, and $\Delta_{dp_{m,k}^{(t)} \rightarrow \mathbf{p}_k^{(t)}}(\mathbf{p}_k^{(t)})$ can be approximated by a Gaussian distribution, i.e.,

$$\Delta_{xp_{m,k}^{(t)} \rightarrow \mathbf{p}_k^{(t)}}(\mathbf{p}_k^{(t)}) \Delta_{yp_{m,k}^{(t)} \rightarrow \mathbf{p}_k^{(t)}}(\mathbf{p}_k^{(t)}) \Delta_{dp_{m,k}^{(t)} \rightarrow \mathbf{p}_k^{(t)}}(\mathbf{p}_k^{(t)}) = \mathcal{N}(\mathbf{p}_k^{(t)}; \mathbf{m}_{m,k}^{(t)}, \mathbf{C}_{m,k}^{(t)}). \quad (36)$$

$\mathbf{m}_{m,k}^{(t)}$ and $\mathbf{C}_{m,k}^{(t)}$ in (36) is given by

$$\mathbf{m}_{m,k}^{(t)} = \mathbf{p}_{R,m} + d_{m,k}^{(t)} \mathbf{E}_m \mathbf{v}_{m,k}^{(t)}, \quad (37a)$$

$$\mathbf{C}_{m,k}^{(t)} = \mathbf{E}_{m,k} \text{diag}(\mathbf{u}_{m,k}^{(t)}) \mathbf{E}_{m,k}^T, \quad (37b)$$

where $d_{m,k}^{(t)} = c_0(\mu_{\zeta_{m,k}^{(t)} \rightarrow dp_{m,k}^{(t)}} - \tau_m)$, $\mathbf{E}_m = [\mathbf{e}_{m,x}, \mathbf{e}_{m,y}, \mathbf{e}_{m,z}]$ with $\mathbf{e}_{m,z} = \mathbf{e}_{m,x} \times \mathbf{e}_{m,y}$, $\mathbf{v}_{m,k}^{(t)} = \left[\mu_{\vartheta_{m,k,x}^{(t)} \rightarrow xp_{m,k}^{(t)}} + \phi_{m,x}, \mu_{\vartheta_{m,k,y}^{(t)} \rightarrow yp_{m,k}^{(t)}} + \phi_{m,y}, \left(1 - (\mu_{\vartheta_{m,k,x}^{(t)} \rightarrow xp_{m,k}^{(t)}} + \phi_{m,x})^2 - (\mu_{\vartheta_{m,k,y}^{(t)} \rightarrow yp_{m,k}^{(t)}} + \phi_{m,y})^2 \right)^{\frac{1}{2}} \right]^T$, $\mathbf{E}_m = [\mathbf{e}_{m,x}, \mathbf{e}_{m,y}, \hat{\mathbf{e}}_{m,k}]$ with $\hat{\mathbf{e}}_{m,k} = \mathbf{E}_m \mathbf{v}_{m,k}^{(t)}$, and $\mathbf{u}_{m,k}^{(t)} = \left[\frac{(d_{m,k}^{(t)})^2}{\kappa_{\vartheta_{m,k,x}^{(t)} \rightarrow xp_{m,k}^{(t)}}}, \frac{(d_{m,k}^{(t)})^2}{\kappa_{\vartheta_{m,k,y}^{(t)} \rightarrow yp_{m,k}^{(t)}}}, \frac{c_0^2}{\kappa_{\zeta_{m,k}^{(t)} \rightarrow dp_{m,k}^{(t)}}} \right]$.

Assuming that a Gaussian distribution $p(\mathbf{p}_k^{(0)})$ for each $1 \leq k \leq K$ is provided in the initial frame, all the messages passing along the Markov chain $\{\mathbf{p}_k^{(t)}\}$ are Gaussian messages. Then, $\Delta_{\mathbf{p}_k^{(t)} \rightarrow pp_k^{(t+1)}}(\mathbf{p}_k^{(t)})$ is a Gaussian distribution with mean vector and covariance matrix given by

$$\mathbf{m}_{\mathbf{p}_k^{(t)} \rightarrow pp_k^{(t+1)}} = \mathbf{C}_{\mathbf{p}_k^{(t)} \rightarrow pp_k^{(t+1)}} \left(\sum_{k=1}^K (\mathbf{C}_{m,k}^{(t)})^{-1} \mathbf{m}_{m,k}^{(t)} + \mathbf{C}_{pp_k^{(t)} \rightarrow \mathbf{p}_k^{(t)}}^{-1} \mathbf{m}_{pp_k^{(t)} \rightarrow \mathbf{p}_k^{(t)}} \right), \quad (38a)$$

$$\mathbf{C}_{\mathbf{p}_k^{(t)} \rightarrow pp_k^{(t+1)}}^{-1} = \sum_{k=1}^K (\mathbf{C}_{m,k}^{(t)})^{-1} + \mathbf{C}_{pp_k^{(t)} \rightarrow \mathbf{p}_k^{(t)}}^{-1}. \quad (38b)$$

2) *Messages from $pp_k^{(t+1)}$ to $\mathbf{p}_k^{(t+1)}$* : For $1 \leq k \leq K$,

$$\Delta_{pp_k^{(t+1)} \rightarrow \mathbf{p}_k^{(t+1)}}(\mathbf{p}_k^{(t+1)}) \propto \int_{\mathbf{p}_k^{(t)}} \Delta_{\mathbf{p}_k^{(t)} \rightarrow pp_k^{(t+1)}}(\mathbf{p}_k^{(t)}) p(\mathbf{p}_k^{(t+1)} | \mathbf{p}_k^{(t)}). \quad (39)$$

Given (14), the Gaussian message $\Delta_{pp_k^{(t+1)} \rightarrow \mathbf{p}_k^{(t+1)}}$ is calculated by

$$\mathbf{m}_{pp_k^{(t+1)} \rightarrow \mathbf{p}_k^{(t+1)}} = \mathbf{m}_{\mathbf{p}_k^{(t)} \rightarrow pp_k^{(t+1)}}, \quad (40a)$$

$$\mathbf{C}_{pp_k^{(t+1)} \rightarrow \mathbf{p}_k^{(t+1)}} = \mathbf{C}_{\mathbf{p}_k^{(t)} \rightarrow pp_k^{(t+1)}} + \mathbf{C}_k. \quad (40b)$$

3) *Messages from $\zeta_{m,k}^{(t)}$ to $zz_{m,k}^{(t+1)}$* : Based on the variational inference in Section III-B, the message $\Delta_{\zeta_{m,k}^{(t)} \rightarrow zz_{m,k}^{(t+1)}}(\zeta_{m,k}^{(t)})$ is given by $q(\zeta_m^{(t)})$, i.e., $\Delta_{\zeta_{m,k}^{(t)} \rightarrow zz_{m,k}^{(t+1)}}(\zeta_{m,k}^{(t)}) = \delta(\zeta_{m,k}^{(t)} - \hat{\zeta}_{m,k}^{(t)})$.

4) *Messages from $zz_{m,k}^{(t+1)}$ to $\zeta_{m,k}^{(t+1)}$* : For $1 \leq m \leq M$, $1 \leq k \leq K$,

$$\begin{aligned} \Delta_{zz_{m,k}^{(t+1)} \rightarrow \zeta_{m,k}^{(t+1)}}(\zeta_{m,k}^{(t+1)}) &\propto \int_{\zeta_{m,k}^{(t)}} \Delta_{\zeta_{m,k}^{(t)} \rightarrow zz_{m,k}^{(t+1)}}(\zeta_{m,k}^{(t)}) p(\zeta_{m,k}^{(t+1)} | \zeta_{m,k}^{(t)}) \\ &= p(\zeta_{m,k}^{(t+1)} | \hat{\zeta}_{m,k}^{(t)}), \end{aligned} \quad (41)$$

where $p(\zeta_{m,k}^{(t+1)} | \hat{\zeta}_{m,k}^{(t)})$ is provided in (15).

D. Overall Algorithm

With discussions in the preceding subsections, we summarize our Bayesian multiuser tracking (BMT) algorithm in Algorithm 1. BMT is an online tracking algorithm, where the BS estimates the multiuser positions in each frame by executing the message passing and variational inference. Lines 7-10 of Algorithm 1 correspond to the variational inference. Lines 2-3 and line 15 correspond to the message passing along the Markov chain. As for the initialization of the BMT algorithm in the first pilot frame, we assume that the initial position information of the users is obtained from the Global Positioning System (GPS) with the mean and covariance denoted by $\mathbf{m}_{\mathbf{p}_k^{(0)} \rightarrow pp_k^{(1)}}$ and $\mathbf{C}_{\mathbf{p}_k^{(0)} \rightarrow pp_k^{(1)}}$. The estimation of channel parameters $\{\vartheta_{m,x}^{(t)}, \vartheta_{m,y}^{(t)}, \varsigma_m^{(t)}\}$ are obtained from position estimations $\{\mathbf{m}_{\mathbf{p}_k^{(t)} \rightarrow pp_k^{(t+1)}}\}$ based on geometric constraint (11).

The complexity of the BMT algorithm mainly arises from the variational inference, i.e., lines 7-10 in Algorithm 1. The complexity of calculating $q(\vartheta_{m,k,x}^{(t)})$ and $q(\vartheta_{m,k,y}^{(t)})$ is $\mathcal{O}(K(n_x N_x + n_y N_y))$ where n_x and n_y are the iteration numbers of GDM. The complexity of calculating $q(\varsigma_{m,k}^{(t)})$, $q(\zeta_m^{(t)})$, and $q(\varrho_m^{(t)})$ are respectively $\mathcal{O}(KL^2)$, $\mathcal{O}(K^3 GL)$, and $\mathcal{O}(K^2 GN_R(N_x + N_y))$. Therefore, the overall complexity of BMT is $\mathcal{O}(n_1 MK(n_x N_x + n_y N_y + L^2 + K^2 GL + KGN_R(N_x + N_y)))$, where n_1 is the number of iterations needed in the variational inference.

IV. BAYESIAN CRAMER RAO BOUND

For the deterministic parameter estimation problem, a useful lower bound for the MSE of the unbiased estimator is the Cramer Rao bound (CRB), calculated from the inverse of the Fisher information matrix (FIM). For the random parameter estimation problem as considered in this paper, the BCRB proposed in [31] is desired. In this section, we derive the BCRB for the estimation of the multiuser positions and the channel parameters in a single frame from the BIM. We assume $\zeta_{m,k}^{(t)} = 1$ for all k , m , and t in the derivation. We define two parameter sets involved in the derivation, i.e., $\boldsymbol{\eta}^{(t)} = [(\boldsymbol{\eta}_1^{(t)})^T, \dots, (\boldsymbol{\eta}_K^{(t)})^T]^T$ and $\boldsymbol{\gamma}^{(t)} = [(\boldsymbol{\gamma}_{1,1}^{(t)})^T, (\boldsymbol{\gamma}_{1,2}^{(t)})^T, \dots, (\boldsymbol{\gamma}_{M,K}^{(t)})^T]^T$ where¹

$$\boldsymbol{\eta}_k^{(t)} = [(\mathbf{p}_k^{(t)})^T, \arg \varrho_{1,k}^{(t)}, |\varrho_{1,k}^{(t)}|, \dots, \arg \varrho_{M,k}^{(t)}, |\varrho_{M,k}^{(t)}|]^T, \quad (42a)$$

$$\boldsymbol{\gamma}_{m,k}^{(t)} = [\vartheta_{m,k}^{(t)}, \vartheta_{m,k}^{(t)}, \varsigma_{m,k}^{(t)}, \arg \varrho_{m,k}^{(t)}, |\varrho_{m,k}^{(t)}|]^T. \quad (42b)$$

¹When the LoS path is blocked, i.e., $\zeta_{m,k}^{(t)} = 0$, we remove the correspond parameters $\arg \varrho_{m,k}^{(t)}$ and $|\varrho_{m,k}^{(t)}|$ from the parameter set $\boldsymbol{\eta}_k^{(t)}$ and $\boldsymbol{\gamma}_{m,k}^{(t)}$. The derivation of the BCRB remains the same.

Algorithm 1 BMT Algorithm

Input: Observed signal $\mathbf{y}^{(t,g,l)}$ for $1 \leq t \leq T$, $1 \leq g \leq G$, $1 \leq l \leq L$, initial user position estimation $\mathbf{m}_{\mathbf{p}_k^{(0)} \rightarrow pp_k^{(1)}}$ with its covariance matrix $\mathbf{C}_{\mathbf{p}_k^{(0)} \rightarrow pp_k^{(1)}}$ for $1 \leq k \leq K$.

Output: Position estimations $\{\mathbf{m}_{\mathbf{p}_k^{(t)} \rightarrow pp_k^{(t+1)}}\}$, cascaded channel path gain estimations $\{\hat{\varrho}_{m,k}^{(t)}\}$, and blockage estimations $\{\hat{\zeta}_k^{(t)}\}$ for $1 \leq t \leq T$, $1 \leq k \leq K$, $1 \leq m \leq M$.

```

1: for  $t = 1$  to  $T$  do
2:   For  $\forall k$ , calculate  $\mathbf{m}_{pp_k^{(t)} \rightarrow \mathbf{p}_k^{(t)}}$  and  $\mathbf{C}_{pp_k^{(t)} \rightarrow \mathbf{p}_k^{(t)}}$  by (40).
3:   For  $\forall m, k$ , calculate  $\Delta_{zz_{m,k}^{(t)} \rightarrow \zeta_{m,k}^{(t)}}(\zeta_{m,k}^{(t)})$  by (41).
4:   for  $m = 1$  to  $M$  do
5:     For  $\forall g, l$ , calculate  $\Delta_{[\mathbf{r}_{g,l}^{(t)}]_m \rightarrow h_m^{(t)}}([\mathbf{r}_{g,l}^{(t)}]_m)$  by (19).
6:     For  $\forall k$ , calculate  $\Delta_{xp_{m,k}^{(t)} \rightarrow \vartheta_{m,k,x}^{(t)}}(\vartheta_{m,k,x}^{(t)})$ ,  $\Delta_{yp_{m,k}^{(t)} \rightarrow \vartheta_{m,k,y}^{(t)}}(\vartheta_{m,k,y}^{(t)})$  and  $\Delta_{dp_{m,k}^{(t)} \rightarrow \zeta_{m,k}^{(t)}}(\zeta_{m,k}^{(t)})$ .
7:     repeat
8:       For  $\forall k$ , calculate  $q(\vartheta_{m,k,x}^{(t)})$  and  $q(\vartheta_{m,k,y}^{(t)})$ .
9:       For  $\forall k$ , calculate  $q(\zeta_{m,k}^{(t)})$ .
10:      Calculate  $q(\zeta_m^{(t)})$ .
11:      Calculate  $q(\varrho_m^{(t)})$ .
12:     until stopping criterion
13:     For  $\forall k$ , calculate  $\Delta_{\vartheta_{m,k,x}^{(t)} \rightarrow xp_{m,k}^{(t)}}(\vartheta_{m,k,x}^{(t)})$ ,  $\Delta_{\vartheta_{m,k,y}^{(t)} \rightarrow yp_{m,k}^{(t)}}(\vartheta_{m,k,y}^{(t)})$  and  $\Delta_{\zeta_{m,k}^{(t)} \rightarrow dp_{m,k}^{(t)}}(\zeta_{m,k}^{(t)})$ .
14:   end for
15:   For  $\forall k$ , Calculate  $\mathbf{m}_{\mathbf{p}_k^{(t)} \rightarrow pp_k^{(t+1)}}$  and  $\mathbf{C}_{\mathbf{p}_k^{(t)} \rightarrow pp_k^{(t+1)}}$  by (38).
16: end for
17: return  $\{\mathbf{m}_{\mathbf{p}_k^{(t)} \rightarrow pp_k^{(t+1)}}\}$ ,  $\{\hat{\varrho}_{m,k}^{(t)}\}$ , and  $\{\hat{\zeta}_m^{(t)}\}$  for  $1 \leq t \leq T$ ,  $1 \leq k \leq K$ ,  $1 \leq m \leq M$ .

```

The BCRB for the parameter set $\boldsymbol{\eta}^{(t)}$ in each frame t is calculated from the BIM denoted by $\boldsymbol{\Lambda}_B^{(t)}$. It is shown in [32] that the BIM for discrete-time filtering obeys the recursion

$$\boldsymbol{\Lambda}_B^{(t)} = \boldsymbol{\Lambda}^{(t)} + \mathbf{G}_{22}^{(t)} + \mathbf{G}_{21}^{(t)}(\boldsymbol{\Lambda}_B^{(t-1)} + \mathbf{G}_{11}^{(t)})^{-1}\mathbf{G}_{12}^{(t)}, \quad (43)$$

where $\boldsymbol{\Lambda}^{(t)}$ is the FIM of parameter set $\boldsymbol{\eta}^{(t)}$ and the other items are defined as

$$\mathbf{G}_{ij}^{(t)} = \mathbb{E} \left[-\frac{\partial^2 \log p(\boldsymbol{\eta}^{(t)} | \boldsymbol{\eta}^{(t-1)})}{\partial \boldsymbol{\eta}^{(t+i-2)} \partial (\boldsymbol{\eta}^{(t+j-2)})^T} \right], \text{ for } i, j \in \{1, 2\}, \quad (44)$$

where the expectation is taken over $p(\boldsymbol{\eta}^{(t)}, \boldsymbol{\eta}^{(t-1)})$. Given the conditional probability (14) and the conditional independence between $\varrho_{m,k}^{(t)}$ and $\varrho_{m,k}^{(t-1)}$, the nonzero submatrices in (44) are

$$\mathbb{E} \left[-\frac{\partial^2 \log p(\boldsymbol{\eta}^{(t)} | \boldsymbol{\eta}^{(t-1)})}{\partial \mathbf{p}_k^{(t+i-2)} \partial (\mathbf{p}_k^{(t+j-2)})^T} \right] = (-1)^{i+j} \mathbf{C}_k^{-1}, \text{ for } i, j \in \{1, 2\}. \quad (45)$$

Given the complex-Gaussian-noise-disturbed received signal in (7), the FIM of parameter set $\boldsymbol{\eta}^{(t)}$ is calculated by [33]

$$\boldsymbol{\Lambda}^{(t)} = \frac{2}{\nu} \sum_{g=1}^G \sum_{l=1}^L \operatorname{Re} \left\{ \left(\frac{\partial \mathbf{m}^{(t,g,l)}}{\partial \boldsymbol{\eta}^{(t)}} \right)^H \left(\frac{\partial \mathbf{m}^{(t,g,l)}}{\partial \boldsymbol{\eta}^{(t)}} \right) \right\}, \quad (46)$$

$$\stackrel{(a)}{=} \frac{2}{\nu} (\mathbf{T}^{(t)})^T \sum_{g=1}^G \sum_{l=1}^L \operatorname{Re} \left\{ \left(\frac{\partial \mathbf{r}_{g,l}^{(t)}}{\partial \boldsymbol{\gamma}^{(t)}} \right)^H \mathbf{A}_B^H(\boldsymbol{\theta}) \mathbf{A}_B(\boldsymbol{\theta}) \left(\frac{\partial \mathbf{r}_{g,l}^{(t)}}{\partial \boldsymbol{\gamma}^{(t)}} \right) \right\} \mathbf{T}^{(t)}, \quad (47)$$

where $\stackrel{(a)}{=}$ utilizes the chain rule, $\mathbf{m}^{(t,g,l)} = \mathbf{A}_B(\boldsymbol{\theta}) \mathbf{r}_{g,l}^{(t)}$ is the noise-free version of the received signal $\mathbf{y}^{(t,g,l)}$, and $\mathbf{T}^{(t)} = \frac{\partial \boldsymbol{\gamma}^{(t)}}{\partial \boldsymbol{\eta}^{(t)}}$ with the nonzero entries being calculated based on (11) given by

$$\frac{\partial \vartheta_{m,k,x}^{(t)}}{\partial \mathbf{p}_k^{(t)}} = \frac{\mathbf{e}_{m,x} - (\mathbf{e}_{m,k}^{(t)})^T \mathbf{e}_{m,x} \mathbf{e}_{m,k}^{(t)}}{\|\mathbf{p}_k^{(t)} - \mathbf{p}_{R,m}\|^2}, \quad (48a)$$

$$\frac{\partial \vartheta_{m,k,y}^{(t)}}{\partial \mathbf{p}_k^{(t)}} = \frac{\mathbf{e}_{m,y} - (\mathbf{e}_{m,k}^{(t)})^T \mathbf{e}_{m,y} \mathbf{e}_{m,k}^{(t)}}{\|\mathbf{p}_k^{(t)} - \mathbf{p}_{R,m}\|^2}, \quad (48b)$$

$$\frac{\partial \varsigma_{m,k}^{(t)}}{\partial \mathbf{p}_k^{(t)}} = \frac{\mathbf{e}_{m,k}^{(t)}}{c_0}, \quad (48c)$$

$$\frac{\partial \arg \varrho_{m,k}^{(t)}}{\partial \arg \varrho_{m,k}^{(t)}} = 1, \quad \frac{\partial |\varrho_{m,k}^{(t)}|}{\partial |\varrho_{m,k}^{(t)}|} = 1, \quad (48d)$$

where $\mathbf{e}_{m,k}^{(t)} = \frac{\mathbf{p}_k^{(t)} - \mathbf{p}_{R,m}}{\|\mathbf{p}_k^{(t)} - \mathbf{p}_{R,m}\|}$ is the unit vector pointing from the k -th RIS to the m -th user. The nonzero entries of $\frac{\partial \mathbf{r}_{g,l}^{(t)}}{\partial \boldsymbol{\gamma}^{(t)}}$ are calculated based on (9) given by

$$\frac{\partial [\mathbf{r}_{g,l}^{(t)}]_m}{\partial \vartheta_{m,k,x}^{(t)}} = x_k^{(t,l)} \varrho_{m,k}^{(t)} [\mathbf{a}_L(\varsigma_{m,k}^{(t)})]_l (\boldsymbol{\omega}_m^{(t,g)})^T \frac{\partial \mathbf{a}_x(\vartheta_{m,k,x}^{(t)})}{\partial \vartheta_{m,k,x}^{(t)}} \otimes \mathbf{a}_y(\vartheta_{m,k,y}^{(t)}), \quad (49a)$$

$$\frac{\partial [\mathbf{r}_{g,l}^{(t)}]_m}{\partial \vartheta_{m,k,y}^{(t)}} = x_k^{(t,l)} \varrho_{m,k}^{(t)} [\mathbf{a}_L(\varsigma_{m,k}^{(t)})]_l (\boldsymbol{\omega}_m^{(t,g)})^T \mathbf{a}_x(\vartheta_{m,k,x}^{(t)}) \otimes \frac{\partial \mathbf{a}_y(\vartheta_{m,k,y}^{(t)})}{\partial \vartheta_{m,k,y}^{(t)}}, \quad (49b)$$

$$\frac{\partial [\mathbf{r}_{g,l}^{(t)}]_m}{\partial \varsigma_{m,k}^{(t)}} = x_k^{(t,l)} \varrho_{m,k}^{(t)} \left[\frac{\partial \mathbf{a}_L(\varsigma_{m,k}^{(t)})}{\partial \varsigma_{m,k}^{(t)}} \right]_l (\boldsymbol{\omega}_m^{(t,g)})^T \mathbf{a}_x(\vartheta_{m,k,x}^{(t)}) \otimes \mathbf{a}_y(\vartheta_{m,k,y}^{(t)}), \quad (49c)$$

$$\frac{\partial [\mathbf{r}_{g,l}^{(t)}]_m}{\partial \arg \varrho_{m,k}^{(t)}} = j x_k^{(t,l)} \varrho_{m,k}^{(t)} [\mathbf{a}_L(\varsigma_{m,k}^{(t)})]_l (\boldsymbol{\omega}_m^{(t,g)})^T \mathbf{a}_x(\vartheta_{m,k,x}^{(t)}) \otimes \mathbf{a}_y(\vartheta_{m,k,y}^{(t)}), \quad (49d)$$

$$\frac{\partial [\mathbf{r}_{g,l}^{(t)}]_m}{\partial |\varrho_{m,k}^{(t)}|} = x_k^{(t,l)} \frac{\varrho_{m,k}^{(t)}}{|\varrho_{m,k}^{(t)}|} [\mathbf{a}_L(\varsigma_{m,k}^{(t)})]_l (\boldsymbol{\omega}_m^{(t,g)})^T \mathbf{a}_x(\vartheta_{m,k,x}^{(t)}) \otimes \mathbf{a}_y(\vartheta_{m,k,y}^{(t)}). \quad (49e)$$

The BCRB of the parameter estimation $\hat{\boldsymbol{\eta}}^{(t)}$ is given by

$$\mathbb{E}[(\hat{\boldsymbol{\eta}}^{(t)} - \boldsymbol{\eta}^{(t)})(\hat{\boldsymbol{\eta}}^{(t)} - \boldsymbol{\eta}^{(t)})] \succeq (\boldsymbol{\Lambda}_B^{(t)})^{-1}. \quad (50)$$

As for the BCRB of channel parameters $\vartheta_{m,k}^{(t)}$, $\vartheta_{m,k}^{(t)}$, and $\varsigma_{m,k}^{(t)}$, we apply the parameter transformation and obtain the BCRB of parameter estimation $\hat{\boldsymbol{\gamma}}^{(t)}$ given by

$$\mathbb{E}[(\hat{\boldsymbol{\gamma}}^{(t)} - \boldsymbol{\gamma}^{(t)})(\hat{\boldsymbol{\gamma}}^{(t)} - \boldsymbol{\gamma}^{(t)})] \succeq \mathbf{T}^{(t)}(\boldsymbol{\Lambda}_B^{(t)})^{-1}(\mathbf{T}^{(t)})^T. \quad (51)$$

The BCRB acts as a benchmark for our BMT algorithm. In the next section, we design the PBF of multiple RISs based on the derived BCRB.

V. PASSIVE BEAMFORMING DESIGN

To enable high-precision multiuser tracking, the PBF vectors need to be appropriately designed. In (10), the matrix $\mathbf{W}_m^{(t)} \in \mathbb{C}^{N_R \times G}$ collects the PBF vector of the m -th RIS over G OFDM symbols regarded as a measurement matrix. Since the BCRB provides a metric for evaluating the multiuser localization performance in each frame, we minimize the BCRB of the user positions $\{\mathbf{p}_k^{(t)}\}$ by optimizing the PBF of the RISs. The optimization problem in the t -th frame is formulated as

$$\begin{aligned} \text{(P1)} : \quad & \min_{\{\mathbf{W}_m^{(t)}\}_{m=1}^M} \sum_{j \in \mathcal{R}} \left[\left(\boldsymbol{\Lambda}_B^{(t)} (\{\mathbf{W}_m^{(t)}\}_{m=1}^M; \boldsymbol{\eta}^{(t)}) \right)^{-1} \right]_{j,j} \\ \text{s.t.} \quad & |[\mathbf{W}_m^{(t)}]_{n,g}| = 1, \text{ for } 1 \leq m \leq M, 1 \leq n \leq N_R, 1 \leq g \leq G, \end{aligned}$$

where \mathcal{R} indexes the position variables $\{\mathbf{p}_k^{(t)}\}$ in the parameter set $\boldsymbol{\eta}^{(t)}$ and $|[\mathbf{W}_m^{(t)}]_{n,g}| = 1$ is the unit modulus constraint of the RIS phase shift. Note that the objective function in (P1) is parameterized by $\boldsymbol{\eta}^{(t)}$ which is not available in practice. We utilize the estimations in the previous frame and reformulate the objective function in (P1) as

$$\mathbb{E} \left[\sum_{j \in \mathcal{R}} \left[\left(\boldsymbol{\Lambda}_B^{(t)} (\{\mathbf{W}_m^{(t)}\}_{m=1}^M; \boldsymbol{\eta}^{(t)}) \right)^{-1} \right]_{j,j} \right], \quad (52)$$

where the expectation is taken over $\Delta_{pp_k^{(t)} \rightarrow \mathbf{p}_k^{(t)}}(\mathbf{p}_k^{(t)})$ with $\boldsymbol{\varrho}_m^{(t)}$ fixing by the mean of surrogate pdf $q(\boldsymbol{\varrho}_m^{(t-1)})$. In the approximated posterior distribution $q(\boldsymbol{\varrho}_m^{(t-1)})$ given in (30), the estimation of cascaded channel path gain $\varrho_{m,k}^{(t-1)}$ is zero when the LoS path is blocked, i.e., $q(\varrho_{m,k}^{(t-1)} | \varsigma_{m,k}^{(t-1)} = 0) = \delta(\varrho_{m,k}^{(t-1)})$. Without special design, the beamforming design in (P1) neglects these blocked

TABLE II
SYSTEM PARAMETERS

Parameter	Value
λ	10.7 mm
G	15
L	40
f_s	250 kHz
N_B	32
(N_x, N_y)	(10, 10)
\mathbf{p}_B	(-20 m, 0 m, 0 m)
\mathbf{e}_B	(0, 1, 0)
$\mathbf{p}_{R,i}$	(0 m, 20 m, 10 m), (0 m, -20 m, 10 m)
$\mathbf{e}_{R,i,x}$	(1, 0, 0), (-1, 0, 0)
$\mathbf{e}_{R,i,y}$	(0, 0, 1), (0, 0, 1)

paths even if they are no longer blocked in subsequent frames which results in the BMT algorithm not being able to exploit all the geometric constraints. Following the common free space path loss model, we substitute these zero estimations of $\delta(\varrho_{m,k}^{(t-1)})$ by

$$q(\varrho_{m,k}^{(t-1)} | \zeta_{m,k}^{(t-1)} = 0) = \delta \left(\varrho_{m,k}^{(t-1)} - \frac{\lambda^2 e^{-j \frac{2\pi}{\lambda} \left(\|\mathbf{p}_{R,m} - \mathbf{m}_{pp_k^{(t)} \rightarrow \mathbf{p}_k^{(t)}}\|_2 + \|\mathbf{p}_B - \mathbf{p}_{R,m}\|_2 \right)}}{16\pi^2 \|\mathbf{p}_{R,m} - \mathbf{m}_{pp_k^{(t)} \rightarrow \mathbf{p}_k^{(t)}}\|_2 \|\mathbf{p}_B - \mathbf{p}_{R,m}\|_2} \right). \quad (53)$$

It is difficult to explicitly carry out the expectation in (52). We use the sample average to approximate the expectation calculation. In addition, we directly optimize the phase shifts of reflecting elements for RISs and obtain the optimization problem as

$$(P2) : \min_{\{\varphi_{m,n}^{(t,g)}\}} \frac{1}{N_s} \sum_{i=1}^{N_s} \sum_{j \in \mathcal{R}} \left[\left(\Lambda_B^{(t)}(\{\varphi_{m,n}^{(t,g)}\}; \boldsymbol{\eta}^{(t)}) \right)^{-1} \right]_{j,j},$$

where $\varphi_{m,n}^{(t,g)} = \arg[\mathbf{W}_m^{(t)}]_{n,g}$, $\mathbf{p}_k^{(t)}$ in parameter set $\boldsymbol{\eta}^{(t)}$ is sampled from $\Delta_{pp_k^{(t)} \rightarrow \mathbf{p}_k^{(t)}}(\mathbf{p}_k^{(t)})$ for each k , and N_s is the number of samples. Due to the non-convexity of the objective function, the global optimal of (P2) is difficult to be found. We use the GDM to obtain a local minimum of (P2). In each iterative search of GDM, we use the Armijo rule to determine the step size. In the first frame, the gradient descent search starts from a random phase shift setting $\{\varphi_{m,n}^{(0,g)}\}$. In any frame t , the gradient descent search starts from the optimized phase shifts setting in the preceding frame $t - 1$.

VI. NUMERICAL RESULTS

In this section, we conduct numerical experiments to assess the performance of the BMT algorithm proposed in Section III with different system settings, compared with the BCRB derived in Section IV. We execute the BMT algorithm under the PBF designed in Section V as well as other state-of-art PBF designs.

A. Settings of Numerical Experiment

In the numerical experiments, the main parameter settings of the multi-RIS aided MIMO-OFDM systems are listed in Table II, unless otherwise specified. There are $K = 3$ users in the system and the trajectory of each user is generated based on the conditional probability $p(\mathbf{p}_k^{(t)} | \mathbf{p}_k^{(t-1)}) = \mathcal{N}(\mathbf{p}_k^{(t)}; \mathbf{p}_k^{(t-1)}, \mathbf{C}_p)$ with $\mathbf{C}_p = \text{diag}([0.03, 0.03, 0.03]^T)$. The initial location of users $\{\mathbf{p}_k^{(0)}\}_{k=1}^3$ are set to $(-5 \text{ m}, 0 \text{ m}, 3.5 \text{ m})$, $(10 \text{ m}, 10 \text{ m}, 1 \text{ m})$, and $(10 \text{ m}, -10 \text{ m}, 1 \text{ m})$. Each trajectory contains $T = 300$ discrete user positions. We generate the binary variables $\zeta_{m,k}^{(t)}$ based on the birth and death process in (15) with $p_{l,m,k}^{(t)} = 0.9$ and $p_{d,m,k}^{(t)} = 0.05$, given the initialization $\zeta_{m,k}^{(0)} = 1$ for all m, k and t . Given the position of the BS, the RISs, and the users, we generate the complex channel path gains $\rho_{m,k}^{(t)}$ and ρ_m by following the free space path loss model and generate $\varrho_{m,k}^{(t)}$ by

$$\varrho_{m,k}^{(t)} = \zeta_{m,k}^{(t)} \frac{\lambda^2 e^{-j\frac{2\pi}{\lambda} (\|\mathbf{p}_{R,m} - \mathbf{p}_k^{(t)}\|_2 + \|\mathbf{p}_B - \mathbf{p}_{R,m}\|_2)}}{16\pi^2 \|\mathbf{p}_{R,m} - \mathbf{p}_k^{(t)}\|_2 \|\mathbf{p}_B - \mathbf{p}_{R,m}\|_2}. \quad (54)$$

The pilot signals of different users are orthogonally set by $\mathbf{x}_k = \mathbf{a}_L(\frac{k}{f_s})$. We evaluate the BMT algorithm performance by the RMSE of user localization and the success rate of $\zeta_{m,k}^{(t)}$ estimation averaging from 20 independently generated trajectories.

B. Results and Discussions

1) *Effect of User Mobility:* We first investigate the impact of user mobility on the performance of the BMT algorithm. In the trajectories generation, user mobility is characterized by the covariance matrix \mathbf{C}_p . Given $\mathbf{C}_p = \text{diag}([0.03, 0.03, 0.03]^T)$, we have $\mathbb{E} \left[\left\| \mathbf{p}_k^{(t+1)} - \mathbf{p}_k^{(t)} \right\|_2^2 \right] = 0.09$. We generate multiuser trajectories with three different \mathbf{C}_p settings and evaluate the tracking performance. Concretely, \mathbf{C}_p is set by $\mathbf{C}_p = \text{diag}([0.01, 0.01, 0.01]^T)$, $\mathbf{C}_p = \text{diag}([0.03, 0.03, 0.03]^T)$, and $\mathbf{C}_p = \text{diag}([0.05, 0.05, 0.05]^T)$ and are respectively denoted by type 1, type 2 and type 3 in

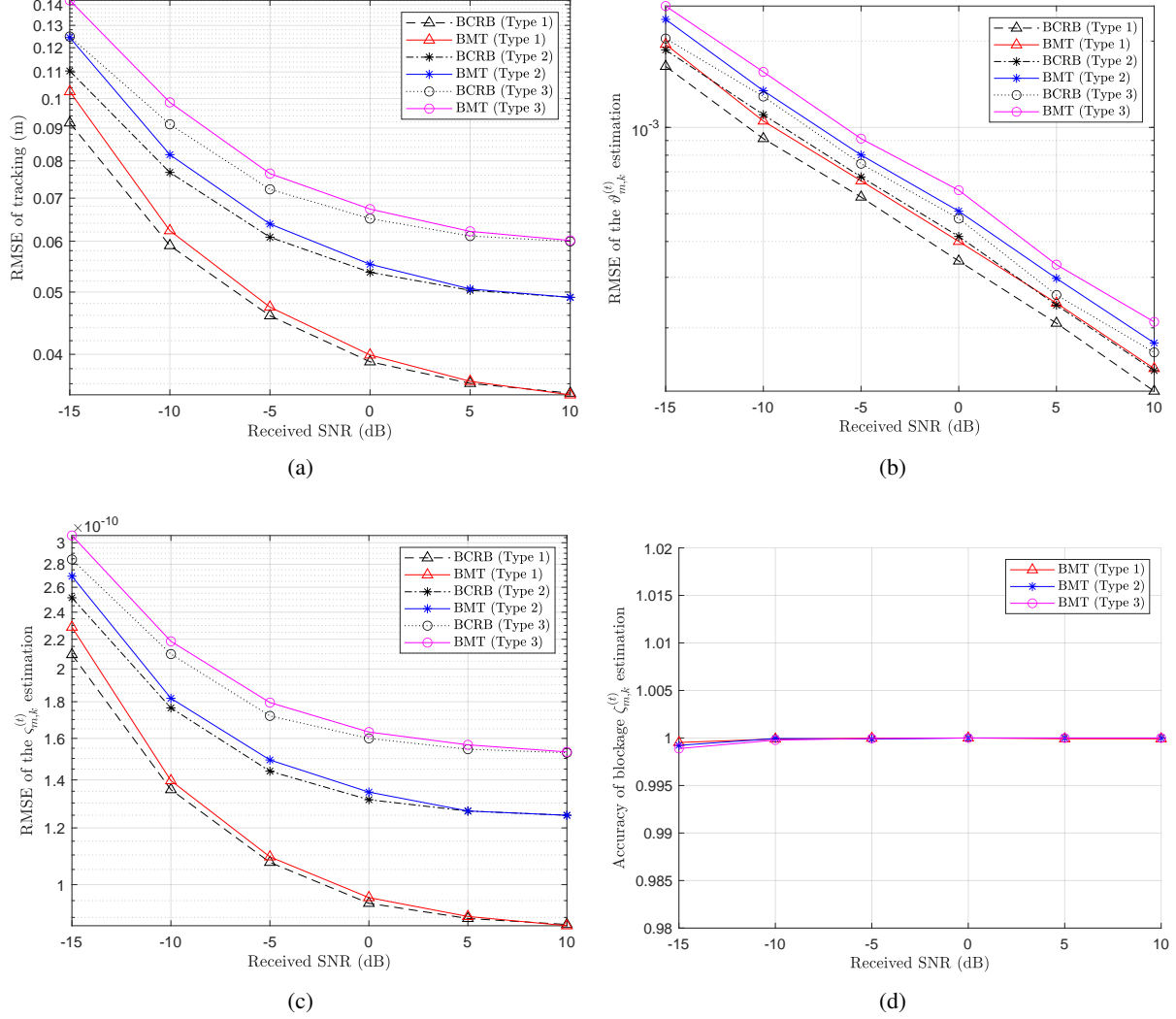


Fig. 3. The BMT algorithm performance v.s. SNR for different user mobility. (a) RMSE of the multiuser position $\mathbf{p}_k^{(t)}$ estimations; (b) RMSE of the $\vartheta_{m,k}^{(t)}$ estimations; (c) RMSE of the $\zeta_{m,k}^{(t)}$ estimations; (d) accuracy of blockage $\zeta_{m,k}^{(t)}$ estimations

Fig. 3. As shown in Fig 3a, the user tracking performance of slow-moving users significantly outperforms fast-moving users while the tracking performances of all three scenarios are close to their respective BCRBs. When executing the BMT algorithm, the stronger the user mobility, the weaker the temporal correlation of the user position, the less information is carried between adjacent frames, and the poorer the algorithm performance. In Fig. 3b, the accuracy of blockage $\zeta_{m,k}^{(t)}$ estimation in the considered SNR range is close to 1. In the following experiments, we no longer evaluate the performance of $\zeta_{m,k}^{(t)}$ estimation since the results are very similar.

2) *Effect of the RIS Number and the Blockage of LoS Path:* To study the effect of the number of RISs, we add a third RIS located in (10 m, 20 m, 5 m) with $\mathbf{e}_{R,i,x} = (1, 0, 0)$ and $\mathbf{e}_{R,i,y} = (0, 0, 1)$

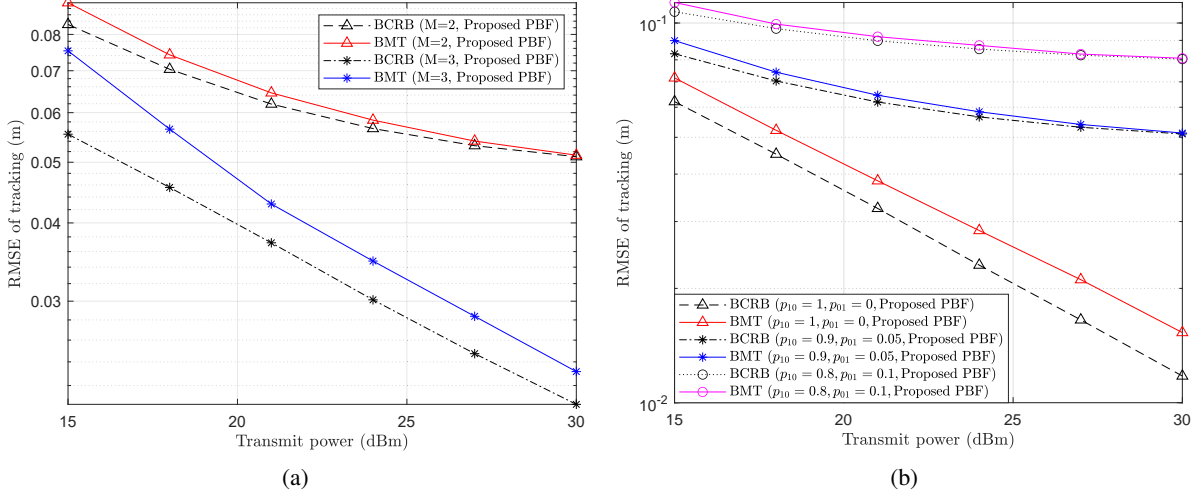


Fig. 4. The BMT algorithm performance v.s. SNR (a) MSE of the multiuser position $\mathbf{p}_k^{(t)}$ estimation for $M = 2$ and $M = 3$; (b) MSE of the multiuser position $\mathbf{p}_k^{(t)}$ estimation with different $p_{l,m,k}^{(t)}$ and $p_{d,m,k}^{(t)}$ settings.

in the MIMO-OFDM system. Fixing the power of interference-plus-noise by $\nu = -125$ dBm, we vary the transmit power and perform the BMT algorithm respectively aided by $M = 2$ RISs and $M = 3$ RISs. The results are shown in Fig. 4a. For both the MSE of multiuser tracking and the BCRB, the additional RIS leads to better tracking performance. To study the effect of the blockage of the LoS path, we generate $\zeta_{m,k}^{(t)}$ based on the birth and death process with different $p_{l,m,k}^{(t)}$ and $p_{d,m,k}^{(t)}$ and evaluate the tracking performance. As shown in Fig. 4b, we achieve the best tracking performance when all the LoS path exists (i.e., $p_{l,m,k}^{(t)} = 1$, $p_{d,m,k}^{(t)} = 0$ for all m , k , and t). As more LoS paths are blocked, the number of available geometric constraints in (11) reduces, which results in progressive deterioration of the tracking performance.

3) *Comparison of Passive Beamforming Methods:* We consider two PBF designs as benchmark schemes, namely, the random PBF design and the discrete Fourier transform (DFT) codebook-based PBF design [34]. For the random PBF design, the RIS phase shift settings are independently drawn from the uniform distribution $U(0, 2\pi)$. For the m -th RIS and k -th user, the DFT codebook is given by

$$\mathbf{W}_{m,k}^{(t)} = [\mathbf{D}^{N_x}]_{1:N_x, (h_{m,k,x}^{(t)} - \frac{H-1}{2}) : (h_{m,k,x}^{(t)} + \frac{H-1}{2})} \otimes [\mathbf{D}^{N_y}]_{1:N_y, (h_{m,k,y}^{(t)} - \frac{H-1}{2}) : (h_{m,k,y}^{(t)} + \frac{H-1}{2})}, \quad (55)$$

where $\mathbf{D}^N \in \mathbb{C}^{N \times N}$ denotes a DFT matrix, $h_{m,k,x}^{(t)} \stackrel{\text{def}}{=} \arg \min_h \|\mathbf{D}^{N_x}\|_{1:N_x, h} - \hat{\mathbf{a}}_x(\vartheta_{m,k,x}^{(t-1)})\|_2$, and $h_{m,k,y}^{(t)} \stackrel{\text{def}}{=} \arg \min_h \|\mathbf{D}^{N_y}\|_{1:N_y, h} - \hat{\mathbf{a}}_y(\vartheta_{m,k,y}^{(t-1)})\|_2$. Based on (55), the DFT codebook for the m -th

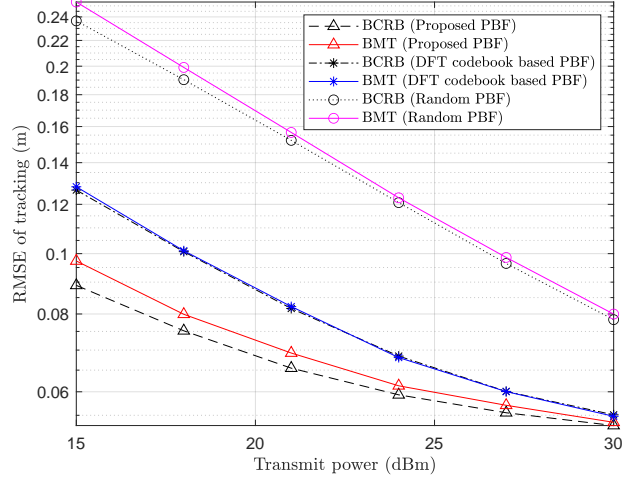


Fig. 5. The BMT algorithm performance v.s. SNR with exploiting different passive beamforming methods. The OFDM overhead is fixed by $G = 12$ for comparing PBF schemes.

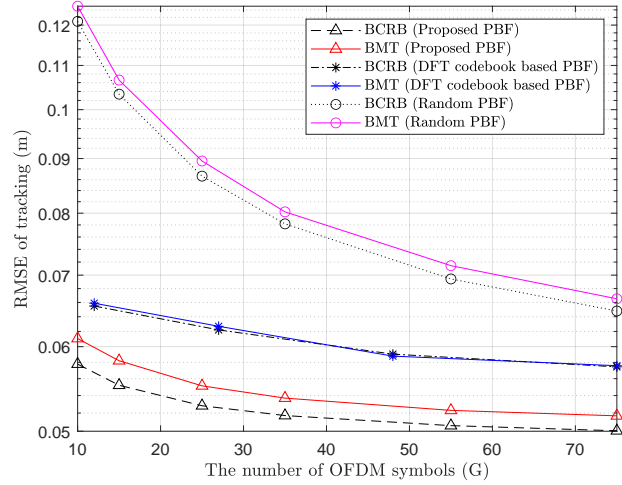


Fig. 6. The BMT algorithm performance v.s. the number of OFDM symbols G by exploiting different passive beamforming methods.

RIS is $\mathbf{W}_m^{(t)} = [\mathbf{W}_{m,1}^{(t)}, \dots, \mathbf{W}_{m,K}^{(t)}] \in \mathbb{C}^{N_R \times KH^2}$. As shown in Fig. 5, the BCRB-based PBF design significantly outperforms the random PBF design and the DFT codebook-based PBF design in multiuser tracking performance.

4) *Effect of the Number of OFDM Symbols:* In this subsection, we set the transmit power by 25 dBm and vary the OFDM symbols overhead $G = [12, 27, 48, 75]$ for the DFT codebook PBF design and $G = [10, 15, 25, 35, 55, 75]$ for the random PBF design and proposed BCRB-based PBF design. The results are shown in Fig. 6, where the RMSE of the multiuser position estimation decreases as the OFDM symbols overhead increases for all three PBF designs. For proposed

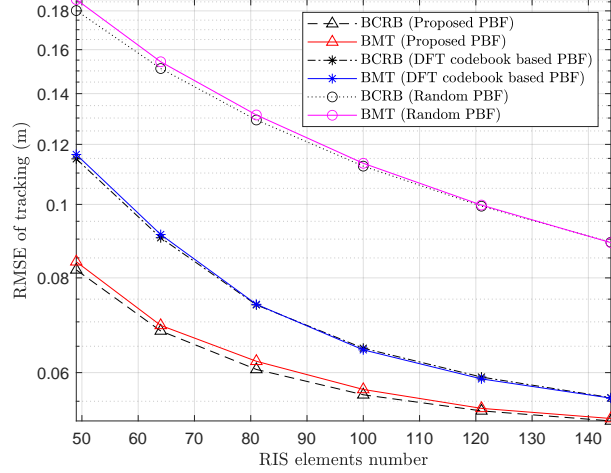


Fig. 7. The BMT algorithm performance v.s. RIS elements number N_R with exploiting different passive beamforming methods. The received noise power is set by -125 dBm. The OFDM overhead is fixed by $G = 12$ for comparing PBF schemes.

BCRB-based PBF and DFT codebook-based PBF, with the RIS elements set by $N_R = 100$ (10×10), the tracking performance is nearly saturated when the OFDM symbols overhead G exceeds 40.

5) *Effect of the Number of RIS Elements:* As shown in Fig. 7, we study the impact of the RIS element number on the multiuser tracking performance. The result shows that the increment of the RIS elements number can significantly improve the tracking performance. More RIS elements number lead to a higher receive SNR since the passive beamforming gain is proportional to the RIS element number. Moreover, with equipping more reflecting elements, the RIS-aided tracking system has a higher angle domain resolution thus leading to more precise multiuser tracking. While the proposed PBF significantly outperforms benchmark schemes when the number of RIS elements is small, the tracking performance gap between DFT codebook-based PBF and proposed PBF reduces when N_R becomes large.

VII. CONCLUSION

In this paper, we studied the multiuser tracking problem in the multi-RIS-aided MIMO-OFDM system. We first built a probability model for multiuser positions and channel parameters by utilizing the geometric relationship of the LoS paths and the temporal correlation of user positions. The blockage of the LoS paths between multiple RIS and users was also considered in our model. Then, we proposed an online Bayesian multiuser tracking algorithm based on the message passing principle where the Gaussian message approximation and variational inference

are exploited to calculate the messages. We developed the BCRB to analyze the performance limits of the tracking problem which further guides the PBF design of the multiple RISs. Numerical simulation results showed that the proposed BMT algorithm can achieve centimeter-level multiuser tracking accuracy and the proposed BCRB-based PBF design outperforms the benchmark PBF schemes in improving the multiuser tracking accuracy.

APPENDIX A DERIVATION OF (26)

The optimal form of $q(\vartheta_{k,x})$ maximizing \mathcal{L} is calculated by [29]

$$\ln q(\vartheta_{k,x}) = \mathbb{E}_{\vartheta_{k,x}} [\ln \Delta(\boldsymbol{\vartheta}_x, \boldsymbol{\vartheta}_y, \boldsymbol{\varsigma}, \boldsymbol{\zeta}, \boldsymbol{\varrho})] + \text{const}, \quad (56)$$

where $\mathbb{E}_{\vartheta_{k,x}}[\cdot]$ denote the expectation over $\frac{q(\boldsymbol{\vartheta}_x, \boldsymbol{\vartheta}_y, \boldsymbol{\varsigma}, \boldsymbol{\zeta}, \boldsymbol{\varrho})}{q(\vartheta_{k,x})}$. We further obtain

$$\begin{aligned} \ln q(\vartheta_{k,x}) &\stackrel{(a)}{=} \ln \Delta_{xp_k \rightarrow \vartheta_{k,x}}(\vartheta_{k,x}) + \mathbb{E}_{\vartheta_{k,x}} \left[\int_{\mathbf{R}} \prod_{g=1}^G \prod_{l=1}^L p(r_{g,l} | \boldsymbol{\vartheta}_x, \boldsymbol{\vartheta}_y, \boldsymbol{\varsigma}_k, \boldsymbol{\varrho}) \Delta_{r_{g,l} \rightarrow h}(r_{g,l}) \right] + \text{const} \\ &\stackrel{(b)}{=} \ln \Delta_{xp_k \rightarrow \vartheta_{k,x}}(\vartheta_{k,x}) - \mathbb{E}_{\vartheta_{k,x}} \left[\left\| \frac{N_B}{\nu} \left[\mathbf{R} - \mathbf{W}^T \sum_{j=1}^K \varrho_j \mathbf{a}_R(\vartheta_{j,x}, \vartheta_{j,y}) \mathbf{x}_j^T \odot \mathbf{a}_L^T(\varsigma_j) \right] \right\|_F^2 \right] + \text{const} \\ &= \ln \Delta_{xp_k \rightarrow \vartheta_{k,x}}(\vartheta_{k,x}) + \frac{2N_B}{\nu} \mathbb{E}_{\vartheta_{k,x}} \left[\text{Re} \left\{ \mathbf{x}_k^T \odot \mathbf{a}_L^T(\varsigma_k) \mathbf{R}^H \mathbf{W}^T \varrho_k \mathbf{a}_R(\vartheta_{k,x}, \vartheta_{k,y}) \right\} \right] \\ &\quad - \frac{2N_B}{\nu} \mathbb{E}_{\vartheta_{k,x}} \left[\text{Re} \left\{ \sum_{j \neq k} \varrho_j^* \varrho_k \mathbf{x}_k^T \odot \mathbf{a}_L^T(\varsigma_k) \mathbf{x}_j^* \odot \mathbf{a}_L^*(\varsigma_j) \mathbf{a}_R^H(\vartheta_{j,x}, \vartheta_{j,y}) \mathbf{W}^* \mathbf{W}^T \mathbf{a}_R(\vartheta_{k,x}, \vartheta_{k,y}) \right\} \right] \\ &\quad - \frac{N_B}{\nu} \mathbb{E}_{\vartheta_{k,x}} \left[\varrho_k^* \varrho_k \mathbf{x}_k^T \odot \mathbf{a}_L^T(\varsigma_k) \mathbf{x}_k^* \odot \mathbf{a}_L^*(\varsigma_k) \mathbf{a}_R^H(\vartheta_{k,x}, \vartheta_{k,y}) \mathbf{W}^* \mathbf{W}^T \mathbf{a}_R(\vartheta_{k,x}, \vartheta_{k,y}) \right] + \text{const}, \quad (57) \end{aligned}$$

where $\stackrel{(a)}{=}$ and $\stackrel{(b)}{=}$ exploit (23) and (19) respectively. Calculating the expectation, we obtain (26).

APPENDIX B CALCULATION OF THE EXPECTATION INVOLVED IN (26) AND (31)

We construct the matrix $\boldsymbol{\Omega}_g \in \mathbb{C}^{N_y \times N_x}$ corresponding to the g -th column of \mathbf{W} satisfying $[\boldsymbol{\Omega}_g]_{i,j} = [\boldsymbol{\omega}_g]_{(j-1)N_y+i}$. We have

$$\begin{aligned} \left\| \mathbf{W}^T \mathbf{a}_R(\vartheta_{k,x}, \vartheta_{k,y}) \right\|_2^2 &= \sum_{g=1}^G \mathbf{a}_R^H(\vartheta_{k,x}, \vartheta_{k,y}) \boldsymbol{\omega}_g^* \boldsymbol{\omega}_g^T \mathbf{a}_R(\vartheta_{k,x}, \vartheta_{k,y}) \\ &\stackrel{(a)}{=} \mathbf{a}_x^H(\vartheta_{k,x}) \sum_{g=1}^G (\boldsymbol{\Omega}_g^H \mathbf{a}_y^*(\vartheta_{k,y}) \mathbf{a}_y^T(\vartheta_{k,y}) \boldsymbol{\Omega}_g) \mathbf{a}_x(\vartheta_{k,x}), \quad (58) \end{aligned}$$

where $\stackrel{(a)}{=}$ utilizes $\boldsymbol{\omega}_g^T \mathbf{a}_R(\vartheta_{k,x}, \vartheta_{k,y}) = \mathbf{a}_y^T(\vartheta_{k,y}) \boldsymbol{\Omega}_g \mathbf{a}_x(\vartheta_{k,x})$. We calculate

$$\mathbb{E}_{q(\vartheta_{k,y}|\mathbf{R})} \left[\left\| \mathbf{W}^T \mathbf{a}_R(\vartheta_{k,x}, \vartheta_{k,y}) \right\|_2^2 \right] = \mathbf{a}_x^H(\vartheta_{k,x}) \sum_{g=1}^G \left(\boldsymbol{\Omega}_g^H \mathbb{E}_{q(\vartheta_{k,y}|\mathbf{R})} \left[\mathbf{a}_y^*(\vartheta_{k,y}) \mathbf{a}_y^T(\vartheta_{k,y}) \right] \boldsymbol{\Omega}_g \right) \mathbf{a}_x(\vartheta_{k,x}), \quad (59)$$

where $\mathbb{E}_{q(\vartheta_{k,y}|\mathbf{R})} \left[\mathbf{a}_y^*(\vartheta_{k,y}) \mathbf{a}_y^T(\vartheta_{k,y}) \right]$ is calculated by $\text{Toep}(\hat{\mathbf{a}}_y^*(\vartheta_{k,y}), \hat{\mathbf{a}}_y^T(\vartheta_{k,y}))$ with $\text{Toep}(\mathbf{u}, \mathbf{v})$ denotes the Toeplitz matrix constructed by setting \mathbf{u} as the first column and setting \mathbf{v} as the first row. A more compact form is obtained as

$$\mathbb{E}_{q(\vartheta_{i,y}|\mathbf{R})} \left[\left\| \mathbf{W}^T \mathbf{a}_R(\vartheta_{i,x}, \vartheta_{i,y}) \right\|_2^2 \right] = 2 \text{Re} \{ \boldsymbol{\beta}_{x,k}^H \mathbf{a}_x(\vartheta_{k,x}) \}, \quad (60)$$

where the n -th term of $\boldsymbol{\beta}_{x,k}$ is $[\boldsymbol{\beta}_{x,k}]_n = \sum_{(i,j) \in \mathcal{C}} \left[\sum_{g=1}^G \left(\boldsymbol{\Omega}_g^H \text{Toep}(\hat{\mathbf{a}}_y^*(\vartheta_{k,y}), \hat{\mathbf{a}}_y^T(\vartheta_{k,y})) \boldsymbol{\Omega}_g \right) \right]_{i,j}$ with $\mathcal{C} = \{(i,j) | 1 \leq i, j \leq N_x, i - j + 1 = n\}$. We further obtain

$$\mathbb{E}_{q(\vartheta_{i,x}|\mathbf{R})q(\vartheta_{i,y}|\mathbf{R})} \left[\left\| \mathbf{W}^T \mathbf{a}_R(\vartheta_{i,x}, \vartheta_{i,y}) \right\|_2^2 \right] = 2 \text{Re} \{ \boldsymbol{\beta}_{x,k}^H \hat{\mathbf{a}}_x(\vartheta_{k,x}) \}. \quad (61)$$

APPENDIX C

DERIVATION OF (36)

Substituting (12) and (33) in (35), we have

$$\begin{aligned} & \ln \left(\Delta_{xp_{m,k}^{(t)} \rightarrow \mathbf{p}_k^{(t)}}(\mathbf{p}_k^{(t)}) \Delta_{yp_{m,k}^{(t)} \rightarrow \mathbf{p}_k^{(t)}}(\mathbf{p}_k^{(t)}) \Delta_{dp_{m,k}^{(t)} \rightarrow \mathbf{p}_k^{(t)}}(\mathbf{p}_k^{(t)}) \right) \\ &= \kappa_{\vartheta_{m,k,x}^{(t)} \rightarrow xp_{m,k}^{(t)}} \cos \left((\mathbf{e}_{m,k}^{(t)})^T \mathbf{e}_{m,x} - \phi_{m,x} - \mu_{\vartheta_{m,k,x}^{(t)} \rightarrow xp_{m,k}^{(t)}} \right) \\ &+ \kappa_{\vartheta_{m,k,y}^{(t)} \rightarrow yp_{m,k}^{(t)}} \cos \left((\mathbf{e}_{m,k}^{(t)})^T \mathbf{e}_{m,y} - \phi_{m,y} - \mu_{\vartheta_{m,k,y}^{(t)} \rightarrow yp_{m,k}^{(t)}} \right) \\ &+ \kappa_{\varsigma_{m,k}^{(t)} \rightarrow dp_{m,k}^{(t)}} \cos \left(\tau_m + \frac{\left\| \mathbf{p}_k^{(t)} - \mathbf{p}_{R,m} \right\|_2}{c_0} - \mu_{\varsigma_{m,k}^{(t)} \rightarrow dp_{m,k}^{(t)}} \right), \end{aligned} \quad (62)$$

where $\mathbf{e}_{m,k}^{(t)} = \frac{\mathbf{p}_k^{(t)} - \mathbf{p}_{R,m}}{\left\| \mathbf{p}_k^{(t)} - \mathbf{p}_{R,m} \right\|}$. The mean of Gaussian distribution in (36) is given by the maximum of (62), the covariance matrix is given by the Hessian matrix at the maximum. Letting each cosine term equal 1, the maximum is obtained as expressed in (37a). We approximate the cosine term in (62) by $\cos(\theta) = 1 - \frac{\theta^2}{2}$ and substitute $\left\| \mathbf{p}_k^{(t)} - \mathbf{p}_{R,m} \right\|$ by $d_{m,k}^{(t)}$. Keeping the quadratic

term of $(\mathbf{p}_k^{(t)} - \mathbf{p}_{R,m})$, we obtain

$$\begin{aligned}
& \ln \left(\Delta_{x_{p_{m,k}^{(t)} \rightarrow \mathbf{p}_k^{(t)}}}(\mathbf{p}_k^{(t)}) \Delta_{y_{p_{m,k}^{(t)} \rightarrow \mathbf{p}_k^{(t)}}}(\mathbf{p}_k^{(t)}) \Delta_{d_{p_{m,k}^{(t)} \rightarrow \mathbf{p}_k^{(t)}}}(\mathbf{p}_k^{(t)}) \right) \\
&= -(\mathbf{p}_k^{(t)} - \mathbf{p}_{R,m})^T \left(\frac{\kappa_{\vartheta_{m,k,x}^{(t)} \rightarrow x_{p_{m,k}^{(t)}}} \mathbf{e}_{m,x} \mathbf{e}_{m,x}^T}{2(d_{m,k}^{(t)})^2} + \frac{\kappa_{\vartheta_{m,k,y}^{(t)} \rightarrow y_{p_{m,k}^{(t)}}} \mathbf{e}_{m,y} \mathbf{e}_{m,y}^T}{2(d_{m,k}^{(t)})^2} \right. \\
&\quad \left. + \frac{\kappa_{\varsigma_{m,k}^{(t)} \rightarrow d_{p_{m,k}^{(t)}}} (\mathbf{p}_k^{(t)} - \mathbf{p}_{R,m})(\mathbf{p}_k^{(t)} - \mathbf{p}_{R,m})^T}{2c_0^2(d_{m,k}^{(t)})^2} \right) (\mathbf{p}_k^{(t)} - \mathbf{p}_{R,m}) + \text{else}. \tag{63}
\end{aligned}$$

Calculating the Hessian matrix at the maximum further yields (37b).

REFERENCES

- [1] H. Wymeersch, D. Shrestha, C. M. de Lima, V. Jainanarayana, B. Richerzhagen, M. F. Keskin, K. Schindhelm, A. Ramirez, A. Wolfgang, M. F. de Guzman *et al.*, “Integration of communication and sensing in 6G: A joint industrial and academic perspective,” in *IEEE PIMRC Workshops*, Sep. 2021, pp. 1–7.
- [2] F. Liu, Y. Cui, C. Masouros, J. Xu, T. X. Han, Y. C. Eldar, and S. Buzzi, “Integrated sensing and communications: Towards dual-functional wireless networks for 6G and beyond,” *IEEE J. Sel. Areas Commun.*, Mar. 2022, early access.
- [3] J. Yang, X. Yang, C.-K. Wen, and S. Jin, “Integrated sensing and communication with multi-domain cooperation,” *arXiv preprint arXiv:2105.03065*, 2021.
- [4] A. Liu, Z. Huang, M. Li, Y. Wan, W. Li, T. X. Han, C. Liu, R. Du, D. K. P. Tan, J. Lu *et al.*, “A survey on fundamental limits of integrated sensing and communication,” *IEEE Commun. Surv. Tutor.*, Feb. 2022, early access.
- [5] H. Wymeersch, J. He, B. Denis, A. Clemente, and M. Juntti, “Radio localization and mapping with reconfigurable intelligent surfaces,” *IEEE Vehicular Technology Magazine*, vol. 15, no. 4, pp. 52–61, Oct. 2020.
- [6] A. Bourdoux, A. N. Barreto, B. van Liempd, C. de Lima, D. Dardari, D. Belot, E.-S. Lohan, G. Seco-Granados, H. Srieddeen, H. Wymeersch *et al.*, “6G white paper on localization and sensing,” *arXiv preprint arXiv:2006.01779*, 2020.
- [7] L. Liu and S. Zhang, “A two-stage radar sensing approach based on MIMO-OFDM technology,” in *Proc. IEEE Global Commun. Conf. (Globecom) Wkshps.*, Dec. 2020, pp. 1–6.
- [8] Q. Wu, S. Zhang, B. Zheng, C. You, and R. Zhang, “Intelligent reflecting surface aided wireless communications: A tutorial,” *IEEE Trans. Commun.*, pp. 3313–3351, Jan. 2021.
- [9] M. Di Renzo, A. Zappone, M. Debbah, M.-S. Alouini, C. Yuen, J. De Rosny, and S. Tretyakov, “Smart radio environments empowered by reconfigurable intelligent surfaces: How it works, state of research, and the road ahead,” *IEEE J. Sel. Areas Commun.*, vol. 38, no. 11, pp. 2450–2525, Nov. 2020.
- [10] X. Yuan, Y.-J. A. Zhang, Y. Shi, W. Yan, and H. Liu, “Reconfigurable-intelligent-surface empowered wireless communications: Challenges and opportunities,” *IEEE Wireless Commun.*, vol. 28, no. 2, pp. 136–143, 2021.
- [11] C. Huang, S. Hu, G. C. Alexandropoulos, A. Zappone, C. Yuen, R. Zhang, M. Di Renzo, and M. Debbah, “Holographic MIMO surfaces for 6G wireless networks: Opportunities, challenges, and trends,” *IEEE Wireless Commun.*, vol. 27, no. 5, pp. 118–125, Jul. 2020.
- [12] Z. Xing, R. Wang, and X. Yuan, “Passive beamforming design for reconfigurable intelligent surface enabled integrated sensing and communication,” *arXiv preprint arXiv:2206.00525*, 2022.

- [13] S. Abeywickrama, R. Zhang, Q. Wu, and C. Yuen, "Intelligent reflecting surface: Practical phase shift model and beamforming optimization," *IEEE Trans. Commun.*, vol. 68, no. 9, pp. 5849–5863, Jun. 2020.
- [14] C. Huang, R. Mo, and C. Yuen, "Reconfigurable intelligent surface assisted multiuser MISO systems exploiting deep reinforcement learning," *IEEE J. Sel. Areas Commun.*, vol. 38, no. 8, pp. 1839–1850, Jun. 2020.
- [15] H. Zhang, H. Zhang, B. Di, K. Bian, Z. Han, and L. Song, "Metalocalization: Reconfigurable intelligent surface aided multi-user wireless indoor localization," *IEEE Trans. Wireless Commun.*, Jun. 2021, early access.
- [16] A. Elzanaty, A. Guerra, F. Guidi, and M.-S. Alouini, "Reconfigurable intelligent surfaces for localization: Position and orientation error bounds," *IEEE Trans. Signal Process.*, vol. 69, pp. 5386–5402, Aug. 2021.
- [17] W. Wang and W. Zhang, "Joint beam training and positioning for intelligent reflecting surfaces assisted millimeter wave communications," *IEEE Trans. Wireless Commun.*, vol. 20, no. 10, pp. 6282–6297, Apr. 2021.
- [18] Y. Lin, S. Jin, M. Matthaiou, and X. You, "Channel estimation and user localization for IRS-assisted MIMO-OFDM systems," *IEEE Trans. Wireless Commun.*, vol. 21, no. 4, pp. 2320–2335, Apr. 2021.
- [19] —, "Conformal IRS-empowered MIMO-OFDM: Channel estimation and environment mapping," *IEEE Trans. Commun.*, vol. 70, no. 7, pp. 4884–4899, Jul. 2022.
- [20] A. Fascista, M. F. Keskin, A. Coluccia, H. Wymeersch, and G. Seco-Granados, "RIS-aided joint localization and synchronization with a single-antenna receiver: Beamforming design and low-complexity estimation," *IEEE J. Sel. Topics Signal Process.*, vol. 16, no. 5, pp. 1141–1156, Aug. 2022.
- [21] B. Teng, X. Yuan, R. Wang, and S. Jin, "Bayesian user localization and tracking for reconfigurable intelligent surface aided MIMO systems," *IEEE J. Sel. Topics Signal Process.*, vol. 16, no. 5, pp. 1040–1054, Aug. 2022.
- [22] Z. Yu, X. Hu, C. Liu, M. Peng, and C. Zhong, "Location sensing and beamforming design for IRS-enabled multi-user ISAC systems," *IEEE Trans. Signal Process.*, vol. 70, pp. 5178–5193, Nov. 2022.
- [23] L. Wei, C. Huang, G. C. Alexandropoulos, C. Yuen, Z. Zhang, and M. Debbah, "Channel estimation for RIS-empowered multi-user MISO wireless communications," *IEEE Trans. Commun.*, vol. 69, no. 6, pp. 4144–4157, Mar. 2021.
- [24] J. He, H. Wymeersch, and M. Juntti, "Channel estimation for RIS-aided mmwave MIMO systems via atomic norm minimization," *IEEE Trans. Wireless Commun.*, vol. 20, no. 9, pp. 5786–5797, Sep. 2021.
- [25] M. R. Akdeniz, Y. Liu, M. K. Samimi, S. Sun, S. Rangan, T. S. Rappaport, and E. Erkip, "Millimeter wave channel modeling and cellular capacity evaluation," *IEEE J. Sel. Areas Commun.*, vol. 32, no. 6, pp. 1164–1179, Jun. 2014.
- [26] D. L. Donoho, A. Maleki, and A. Montanari, "Message-passing algorithms for compressed sensing," *Proc. Nat. Acad. Sci.*, vol. 106, no. 45, pp. 18 914–18 919, Nov. 2009.
- [27] M.-A. Badiu, T. L. Hansen, and B. H. Fleury, "Variational Bayesian inference of line spectra," *IEEE Trans. Signal Process.*, vol. 65, no. 9, pp. 2247–2261, May 2017.
- [28] J. Zhu, Q. Zhang, P. Gerstoft, M.-A. Badiu, and Z. Xu, "Grid-less variational bayesian line spectral estimation with multiple measurement vectors," *Signal Processing*, vol. 161, pp. 155–164, Apr. 2019.
- [29] C. M. Bishop and N. M. Nasrabadi, *Pattern Recognition and Machine Learning*. Springer, 2006, vol. 4, no. 4.
- [30] K. V. Mardia and P. E. Jupp, *Directional Statistics*. John Wiley & Sons, 2009, vol. 494.
- [31] H. L. Van Trees, *Detection, Estimation, and Modulation Theory, Part I: Detection, Estimation, and Linear Modulation Theory*. John Wiley & Sons, 2004.
- [32] P. Tichavsky, C. H. Muravchik, and A. Nehorai, "Posterior Cramér-Rao bounds for discrete-time nonlinear filtering," *IEEE Trans. Signal Process.*, vol. 46, no. 5, pp. 1386–1396, May 1998.
- [33] S. M. Kay, *Fundamentals of Statistical Signal Processing: Estimation Theory*. Prentice-Hall, Inc., 1993.
- [34] S. Noh, M. D. Zoltowski, and D. J. Love, "Multi-resolution codebook and adaptive beamforming sequence design for millimeter wave beam alignment," *IEEE Trans. Wireless Commun.*, vol. 16, no. 9, pp. 5689–5701, Jun. 2017.